Positron annihilation studies on vacancy defects in group IV semiconductors

Katja Kuitunen

Aalto University School of Science and Technology
Faculty of Information and Natural Sciences
Department of Applied Physics
Espoo, Finland

Dissertation for the degree of Doctor of Science in Technology to be presented with due permission of the Faculty of Information and Natural Sciences for public examination and debate in Auditorium E at Aalto University School of Science and Technology (Espoo, Finland) on the 5th of February, 2010, at 13 o'clock.

Dissertations of Department of Applied Physics

Aalto University School of Science and Technology
Faculty of Information and Natural Sciences
ISSN 1797-9595 (print)
ISSN 1797-9609 (online)

Dissertation 159 (2010):
Katja Kuitunen: Positron annihilation studies on vacancy defects in group IV semiconductors

Opponent:
Prof. Anders Hallén, Royal Institute of Technology - KTH

Pre-examiners:
Dos. Tommy Ahlgren, University of Helsinki
Prof. Thierry Bretagnon, Université des Sciences et Techniques du Languedoc

ISBN 978-952-60-3021-0 (print)
ISBN 978-952-60-3022-7 (online)

Picaset Oy
Helsinki 2010

Abstract

Electrical properties of semiconductor materials are greatly influenced by point defects such as vacancies and interstitials. These defects are common and form during the growth and processing of the material. Positron annihilation spectroscopy is a method suitable for detecting and studying vacancy-type lattice defects. In this work, the formation, properties, and annealing of vacancy defects is studied in silicon, silicon-germanium, and germanium.

Defects consisting of a vacancy and one or several donor atoms are one of the most common defects causing electron trapping and deactivation of n-type doping in silicon and silicon-germanium. In this work, the studies in silicon-germanium show that several germanium atoms accumulate around the vacancy-phosphorus (V-P) pair during the annealing of the samples. The increased Ge-decoration pulls the energy level (-/--) down into the band-gap and makes the V-P pair decorated by several Ge atoms an especially effective trap for conduction electrons. The positron trapping in a vacancy surrounded by three As atoms (V-As_3) is studied in highly As-doped Si. The positron detrapping from the V-As_3 defect at high temperatures is observed and a binding energy of 0.27(3) eV of a positron to the V-As_3 complex is determined.

Defects can also be introduced deliberately by neutron-irradiation and ion-implantation. These techniques offer possibilities for studying the generation and annealing of vacancy defects. In this work, neutron-irradiated germanium is studied. Irradiation induced divacancy defects that are stable at room temperature are observed. A negative charge state of a divacancy is found to stabilize the defect even at 400°C. The divacancy is shown to form bigger clusters before the final recovery at 500°C. Finally, B-doping related problems are studied. The results show that He-implantation produces nanovoids that trap interstitials formed during the B-implantation, reducing the implantation related damage. The positron studies on the excimer laser annealed Si support theoretical calculations, which suggest vacancy formation at the maximum melt depth.

Tiivistelmä

Pistevirheitä, kuten vakansseja (puuttuvia atomeja) ja välisija-atomeja syntyy runsaasti puolijohdemateriaalin kasvatuksen ja prosessoinnin seurauksena ja niillä on suuri vaikutus puolijohteiden sähköisiin ominaisuuksiin. Positroniannihilaatiospektroskopia on menetelmä, jolla voidaan havaita ja tutkia vakanssityyppisiä hilavirheitä. Tässä työssä on tutkittu vakanssivirheitä, niiden syntymistä, ominaisuuksia ja toipumista piissä, piigermaniumissa ja germaniumissa.

Virheet, jotka koostuvat vakanssista ja yhdestä tai useammasta donoriatomista, ovat yleisimpiä varauksenkuljettajien määrää vähentävistä virheistä n-tyyppisessä piissä ja piigermaniumissa. Tässä työssä on tutkittu piigermaniumia ja osoitettu, että toivutuksissa vakanssi-fosforiparin (V-P) ympärille kertyvät germaniumatomit aiheuttavat uuden energiatason (-/--) muodostumisen energia-aukkoon, mikä tekee germanium atomien ympäröimästä V-P-parista tehokkaamman elektroneja johtavuusvyöltä vangitsevan virheen. Voimakkaasti As-seostetussa piissä on puolestaan tutkittu positronien loukkuuntumista kolmen As atomin ympäröimään vakanssivirheeseen (V-As_3) ja havaittu positronin karkaaminen V-As_3-virheestä korkeissa lämpötiloissa. Tulosten perusteella on määritetty positronin sidosenergiaksi V-As_3-kompleksiin 0.27(3) eV.

Vakanssivirheitä voidaan tuottaa myös tarkoituksellisesti neutronisäteilytyksellä ja ioni-istutuksella. Nämä menetelmät tarjoavat mahdollisuuden tutkia vakanssien muodostumista ja toipumista. Tässä työssä on tutkittu neutronisäteilytettyä germaniumia ja havaittu säteilytyksessä syntyvän divakanssi-virheitä, jotka ovat stabiileja huoneenlämpötiloissa ja joiden negatiivinen varaustila stabiloi virheen vielä 400°C lämpötilassa. Lisäksi on havaittu divakanssien muodostavan suurikokoisia ryppäitä ennen lopullista toipumistaan 500°C:ssa. Lopuksi on vielä tutkittu B-seostukseen liittyviä ongelmia. Tulokset osoittavat He-säteilytyksen aiheuttavan näytteen pinnan läheisyyteen nanometriluokan aukkoja, jotka vangitsevat B-istutuksessa syntyviä välisija-atomeja ja vähentävät näin implantoinnissa syntyviä vaurioita. Lisäksi positronituloksien perusteella on saatu vahvistusta laskennallisille tuloksille, joiden mukaan laser-toivutus aiheuttaisi sulatetun ja kiteisen piin rajapintaan booria loukkuunnuttavia vakansseja.

Preface

The work for this thesis was conducted between June 2005 and November 2009 in the Department of Applied Physics at the Helsinki University of Technology.

I want to express my gratitude to my instructor Doc. Filip Tuomisto, for his advice and encouragement. I thank Doc. Jonatan Slotte, who has instructed and supported me in this thesis project. I also want to thank the late prof. Kimmo Saarinen for taking me into the Positron Group and for his advisement and prof. Pekka Hautojärvi and prof. Martti Puska for both many fruitful scientific discussions and for facilitating my work at the Laboratory of Physics and the Department of Applied Physics.

I wish to thank both former and current members of the Positron Group. It has been nice working with you! Dr. Klaus Rytsölä and other technical staff also deserve my gratitude for their assistance in multiple technical problems. The financial support from Jenny and Antti Wihuri foundation is gratefully acknowledged.

I want to thank my parents and my brother who have encouraged my interest in science throughout my life. My dear husband Mikko has supported me through all the difficulties of this work. Last but not least, I want to thank my little son Kaarlo, for enlightening my days with his smiles.

Espoo, January 2010

Katja Kuitunen

Contents

Abstract ii
Tiivistelmä iv
Preface vii
Contents viii
List of publications x

1 Introduction **1**

2 Semiconductor physics and defects in semiconductors **4**
2.1 Silicon and germanium 5
2.2 Point defects in semiconductors 7
2.2.1 Vacancy-donor complexes 8
2.2.2 Energetics of vacancy defects 10
2.3 Diffusion 11
2.4 Semiconductor processing and defects 12
2.5 Semiconductor defect characterization methods 14

3 Positron annihilation spectroscopy **17**
3.1 Positrons in solids 17
3.2 Positron lifetime spectroscopy 18
3.3 Doppler-broadening measurement 21
3.4 Measurement setups 22
3.4.1 Measurements using fast positrons 23
3.4.2 Slow positron beam 23

4 Vacancy-donor complexes related to n-type doping in silicon and silicon-germanium **25**

4.1 Positron trapping kinetics in highly As-doped silicon 25

4.1.1 Thermal generation of vacancies 26

4.1.2 Positron trapping at the V-As_3 complex in silicon . . 28

4.2 The E center in silicon-germanium 31

5 Defects in silicon and germanium caused by post-growth processing **36**

5.1 Divacancy clustering in neutron-irradiated germanium 36

5.2 Vacancy clusters in He-implanted silicon 38

5.3 Vacancy generation in ELA processing of silicon 41

6 Summary **44**

Bibliography **46**

List of publications

This thesis consists of an overview and the following publications:

I K. Kuitunen, K. Saarinen, and F. Tuomisto, *Positron trapping kinetics in thermally generated vacancy donor complexes in highly As-doped silicon*, Physical Review B **75**, 045210, pages 1-5 (2007).

II K. Kuitunen, F. Tuomisto, and J. Slotte, *Evidence of a second acceptor state of the E center in* $Si_{1-x}Ge_x$, Physical Review B (BR) **76**, 233202, pages 1-4 (2007).

III K. Kuitunen, F. Tuomisto, J. Slotte, and I. Capan, *Divacancy clustering in neutron irradiated and annealed n-type germanium*, Physical Review B **78**, 033202, pages 1-4 (2008).

IV S. Kilpeläinen, K. Kuitunen, F. Tuomisto, J. Slotte, E. Bruno, S. Mirabella, and F. Priolo, *Vacancy Engineering by He Induced Nanovoids in Crystalline Si*, Semiconductor Science and Technology **24**, 015005, pages 1-4 (2009).

V A. La Magna, V. Privitera, G. Fortunato, M. Cuscunà, B. G. Svensson, E. Monakhov, K. Kuitunen, J. Slotte, and F. Tuomisto, *Vacancy generation in liquid phase epitaxy of Si*, Physical Review B **75**, 235201, pages 1-6 (2007).

The author, Katja Kuitunen (prev. Pennanen), has had an active role in all the phases of the research reported in this thesis. She has been involved in the planning and performing the experiments as well as in the analysis of the experimental data. She has also contributed to the interpretation of the results. The author has written publications I, II and III and performed and written the experimental part in Publ. V. In Publ. IV, the author participated actively in the planning of the experiments, measured some of the He-implanted Si samples and contributed to the interpretation of the results.

Chapter 1

Introduction

The advances in modern electronics are based on constant research and development of semiconductor materials. The qualities required from a good semiconductor material include proper conductivity and carrier mobility, long term stability and low price. Despite extensive research on various other semiconductor materials most of the current technology is based on one group IV semiconductor material, silicon. Silicon has a forbidden energy gap of 1.1 eV separating the electron-filled valence band and empty conduction band at 0 K. Thus, pure silicon at very low temperatures is an insulator and at room temperature a poor conductor. The combination of easy availability and the existence of a stable oxide SiO_2, that can be used as an insulator and a passivation layer, has ensured the success of the material [1].

Another group IV elemental semiconductor is germanium with an energy gap of 0.66 eV at room temperature. The first transistor was made of germanium in 1947 [2], but several supreme properties allowed silicon to conquer the semiconductor market since then. Germanium has, however, many useful qualities, which have led to an increased interest in using germanium either as an alloy with silicon ($Si_{1-x}Ge_x$) or as a pure material. The low effective masses of the charge carriers in germanium lead to high carrier mobilities. In fact, the hole mobility in Ge is higher than in any of the III-V compounds [1]. Germanium is also relatively easy to incorporate into existing Si manufacturing processes due to the structural and chemical

similarities between the two group IV materials and the difference in the band gap energies can be used to adjust the width of the band gap of the two-component alloy [1]. Nowadays strained $Si_{1-x}Ge_x$ layers are used to increase electron and hole mobilities in high performance transistors [1, 3, 4]. The increased mobility is due to the strain caused by the lattice mismatch between Si and Ge. However, the goal of several research groups is to increase the carrier mobilities even further by building the transistor out of pure germanium [5].

The conductivity of semiconductors is controlled by doping the material with impurity atoms. These impurity atoms add charge carriers by donating an electron to the conduction band (donors) or accepting an electron from the valence band and creating a hole (acceptors). A semiconductor is called n-type when electrons carry the charge and p-type when the current is carried by moving holes.

The electrical properties of semiconductor materials are greatly influenced by the existence of point defects, such as vacancies (missing atoms) and vacancy impurity complexes. These defects are common and form during the growth and processing of the material. However, they can also be introduced in a controlled way by irradiation. Point defects can introduce new energy levels into the forbidden band gap. These defect levels can trap charge carriers and thus cause electrical deactivation in semiconductor materials. Removal of point defects can be done by annealing the material at high temperatures, where the defects become mobile. However, the high temperature processes also increase dopant diffusion, which is harmful when trying to achieve very thin dopant regions and high dopant concentrations.

In n-type $Si_{1-x}Ge_x$ the vacancy-donor complexes and divacancies cause electrical deactivation by trapping charge carriers. With increased dopant concentrations that approach the solid solubility limits in modern transistors, these defects form abundantly. Therefore, understanding of the formation, the properties, and the annealing of these defects is very much needed. Vacancies also play a large role in the diffusion and accumulation of impurities. Donor diffusion is either partly or almost completely vacancy mediated, depending on the size of the dopant atom. Boron in Si diffuses interstitially between regular lattice sites but accumulates to areas containing vacancies [6]. Vacancies can also be used to trap harmful self interstitials that cause increased boron diffusion.

In this thesis, vacancy defects in group IV semiconductors, Si, $Si_{1-x}Ge_x$ and Ge are studied by positron annihilation spectroscopy (PAS). This method, based on the detection of the positron-electron annihilation radiation, allows the determination of vacancy size, chemical structure, charge state and concentration [7–10].

First, the vacancy-donor complexes in n-type silicon and $Si_{1-x}Ge_x$ are studied. In Publ. I, V-As_3 defect complex, where the vacancy is surrounded by three arsenic atoms, is investigated. Positron detrapping from V-As_3 at high temperatures is observed and a binding energy of 0.27(3) eV of a positron to the defect is determined. The results explain, why most of the thermally generated vacancies cannot be observed with positrons in highly As-doped Si. In Publ. II, the effect of the increase in the number of Ge atoms around the vacancy-phosphorus (V-P) pair in relaxed phosphorus doped and proton irradiated $Si_{1-x}Ge_x$ is studied. The results show that the increased number of Ge atoms around the V-P pair pulls the second acceptor level (-/- -) down into the band-gap. This makes the Ge-decorated V-P pair an especially effective trap for the conduction electrons.

Much of the properties of radiation induced defects, such as vacancies, in germanium is still unknown. Positron lifetime spectroscopy is used in Publ. III to study neutron irradiated n-type Ge. The formation of a divacancy defect, that is stable at room temperature, is observed, and the negative charge state of a divacancy is found to stabilize the defect even at 400°C. The divacancy is shown to form bigger clusters before the final annealing at 500°C.

Finally, two different methods to control boron-implantation induced damage is studied in Publs. IV and V. In Publ. IV, helium implantation is studied as a means to control B diffusion in crystalline Si. A "nanovoid" region at 100–200 nm below the sample surface is observed and the interstitials created during B-implantation are shown to get trapped in the nanovoids. Thus, the He-implantation is a good tool for reducing the B diffusion. In Publ. V, the positron measurements of excimer laser annealed Si are used to confirm theoretical results that suggest vacancy accumulation at the maximum melt depth during recrystallization followed by subsequent laser pulses. The results offer explanation to the observed build-up in the B concentration at the maximum melting depth.

Chapter 2

Semiconductor physics and defects in semiconductors

In an intrinsic semiconductor at moderate or high temperatures, a fraction of the electrons is thermally excited from the valence band to the conduction band. These electrons leave behind holes in the valence band and the thermally excited electrons and holes carry electric current. The usefulness of the semiconductor materials in modern electronics is, however, based on the fact that the electrical properties of semiconductors can be altered by introducing impurity atoms that can donate electrons to the conduction band or accept them from the valence band. In n-type doping, the concentration of charge carrier electrons is increased by adding impurity atoms with an extra electron to the material. In the case of group IV semiconductors, this is typically achieved with P, As, or Sb atoms. The atoms having one less electron than group IV elements, such as B, are correspondingly acceptors that make the material p-type by increasing the number of charge carrying holes.

Point defects, such as vacancies and interstitials, have a large impact on the electronic properties of the semiconducting material. Vacancies and interstitials can act as compensating donors or acceptors in the material and thus reduce the carrier concentration. This occurs since these defects introduce new electrical levels into the band gap that can trap electrons or holes depending on the defect in question.

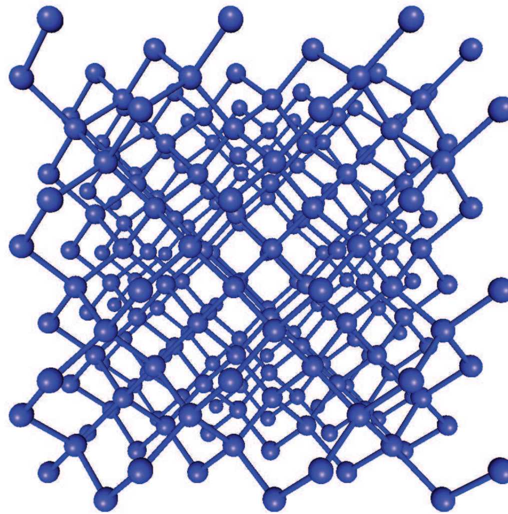

Figure 2.1. *Diamond crystal structure of Si and Ge.*

In this Chapter, the basic principles of semiconductor defect physics are discussed. More details can be found in Refs. [11–15].

2.1 Silicon and germanium

Silicon and germanium are the two elemental semiconductors belonging to the group IV of the chemical table of elements. Thus, they both have four electrons in their outermost electron shell. Both these semiconductor materials have a cubic diamond crystal structure, shown in Fig. 2.1, where each atom is covalently bonded by four bonds to its neighbors.

Silicon is by far the most popular semiconductor used in modern day integrated circuits. The continuing research and development of Si-based materials has enabled the manufacturing of smaller and smaller field-effect transistors (FETs) and thus allowed an increase in computing speed. The "supreme" properties of silicon, compared to the other elemental semiconductor, germanium, include a large band gap, stable oxide, and an extremely low surface-state density [16, 17].

The first transistor was made of germanium, though germanium has been in the shadow of silicon for decades. However, germanium has a higher carrier mobility due to the smaller effective mass of the electrons and holes, which makes it an attractive alternative channel material for p-type metal-oxide-semiconductor field effect transistor (PMOS).

Silicon-germanium ($Si_{1-x}Ge_x$) is a random alloy of Si and Ge. In high performance transistors, strained $Si_{1-x}Ge_x$ layers are used to increase electron and hole mobilities [1, 3, 4]. Due to the similar structural and chemical properties of Si and Ge, $Si_{1-x}Ge_x$ is relatively easy to incorporate into existing Si manufacture processes [1]. The addition of Ge does not change the basic character of the Si band structure with Ge concentrations under 85 %, but it reduces the band gap E_G opening up possibilities for band gap engineering. It also lowers the electron and hole effective masses increasing the charge carrier mobility. The strain produced by the lattice mismatch between Si and Ge also splits the six conduction band valleys of Si in energy and the top of the valence band is split so that the heavy and light hole bands are separated in energy. These changes in the band structure greatly reduce the number of scattering events and cause further increase in the electron and hole mobilities [18, 19]. Relaxed $Si_{1-x}Ge_x$ layers can be achieved *e.g.* by growing a buffer layer with an increasing Ge content. Relaxed $Si_{1-x}Ge_x$ layers have multiple potential applications. They can be used for creating strained Si on relaxed $Si_{1-x}Ge_x$ heterostructures or to achieve relaxed $Si_{1-x}Ge_x$-on-insulator substrates for integrating various device structures [20].

Nowadays the goal of several research groups is to increase the carrier mobilities even further by building the transistor out of pure germanium [5]. The use of germanium still has some problems. First, germanium is expensive and harder to process than Si. Secondly, germanium very easily turns amorphous during ion-implantation, a common process stage. Furthermore, there are difficulties in activating high dopant concentrations in Ge. Above a P concentration of 2×10^{19} cm^{-3}, concentration-enhanced diffusion is observed. The maximum concentration of substitutional P is reached at a concentration of $(5-6)\times10^{19}$ cm^{-3}. This is well below the solid solubility limit and can be due to the formation of electrically inactive V-P complexes [17]. Because Ge was not used in transistors after Si conquered the semiconductor electronics market, not much research on the material properties of germanium has been done. Especially the knowledge on the implantation related

defects and their behavior during thermal processing is lacking.

2.2 Point defects in semiconductors

Point defects in elemental semiconductors can be divided into three groups:

a) Vacancies, in which an atom is missing from a regular lattice site.

b) Interstitial defects, in which an atom occupies the space between regular lattice sites. The interstitial atom can be of the same atomic species as the lattice or it can be an impurity atom.

c) Substitutional impurity atoms.

These defects are point defects in contrast to dislocations that are one-dimensional defects and to two or three dimensional defects such as surfaces, grain boundaries and voids. The simple point defects can also form bigger complexes and clusters. Thus, we have point-like defects such as divacancies, where two vacancies are paired with each other, vacancy clusters, vacancy-impurity or vacancy-interstitial complexes.

The point defects can react with each other through the following reactions [15]:

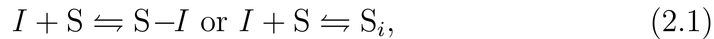

$$I + \mathrm{S} \leftrightharpoons \mathrm{S}{-}I \text{ or } I + \mathrm{S} \leftrightharpoons \mathrm{S}_i, \quad (2.1)$$

$$V + \mathrm{S} \leftrightharpoons \mathrm{S}{-}V, \quad (2.2)$$

$$I + \mathrm{S}{-}V \leftrightharpoons \mathrm{S}, \quad (2.3)$$

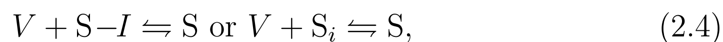

$$V + \mathrm{S}{-}I \leftrightharpoons \mathrm{S} \text{ or } V + \mathrm{S}_i \leftrightharpoons \mathrm{S}, \quad (2.4)$$

$$I + V \leftrightharpoons 0. \quad (2.5)$$

Here S refers to an impurity atom, V to a vacancy, I to an interstitial atom and S_i an impurity atom at an interstitial site. $\mathrm{S}-D$ refers to a complex consisting of an impurity atom and a defect D.

Point defects can introduce electronic levels in the band gap of the semiconductor material. These levels can trap electrons from the conduction band (acceptor levels) or holes from the valence band (donor levels) which

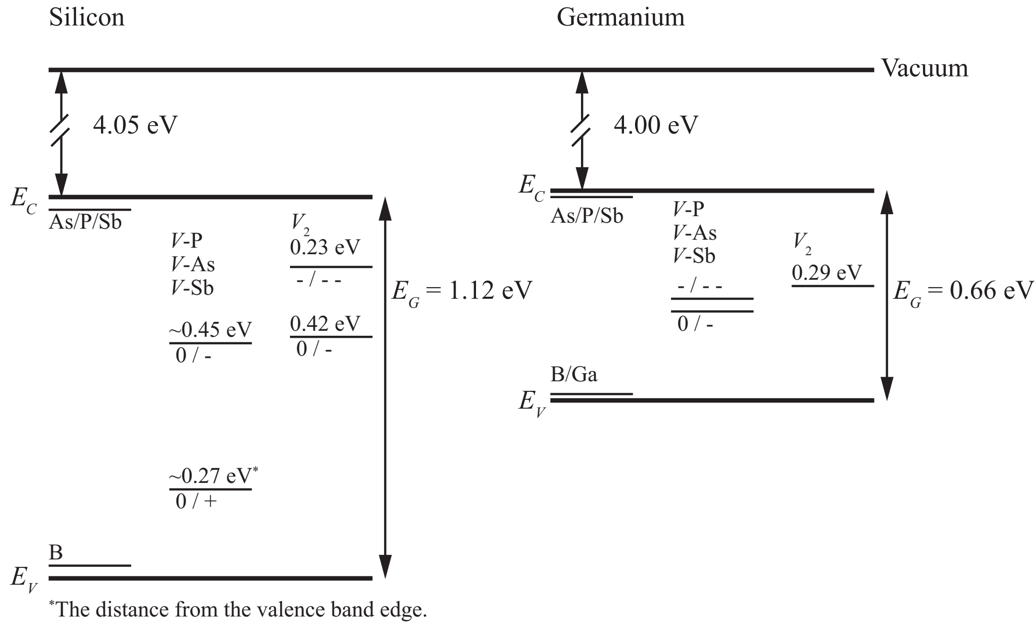

Figure 2.2. *The ionization level positions of some common defects in the Si and Ge band gaps. The values refer to the distance from the conduction band edge E_C, except in the case of the donor level (0/+) of the vacancy-donor pair in Si, where the value refers to the distance from the valence band edge E_V. The exact positions of the vacancy-donor defects depend on the donor atom type. The data is from Refs. [21–23].*

reduce the carrier density. A common way to refer to a particular defect level is to state the charge transition that it corresponds to. Thus, a single acceptor level is referred to as (0/-) and a single donor level as (0/+). As the Fermi level E_F moves upwards, the defects become more negative. Vice versa, the defect charge states become more positive, when E_F moves down towards the valence band. Some common defect types and their ionization level positions in the band gap of Si and Ge are presented in Fig. 2.2.

2.2.1 Vacancy-donor complexes

The miniaturization of the field-effect transistors (FETs) requires increased dopant densities both in the source and drain areas as well as in the chan-

nel [24]. At present, the dopant densities have reached as high as 10^{20} cm^{-3} and fundamental material problems have started to appear. In highly n-type Si, the charge carrier concentration saturates to a value of $\sim 3\times10^{20}$ cm^{-3} regardless of the dopant concentration [15]. This is due to the formation of electrically passive vacancy-donor complexes that is governed by both the thermodynamics and the kinetics during material growth and subsequent processing. In P-doped Ge, the limit of the electron concentration is even lower, $\sim 10^{19}$ cm^{-3} which also might be a result from the formation of vacancy-donor complexes [17]. These defects affect not only the electrical properties of the material but also the migration of impurities and dopants.

Positron annihilation studies in highly As-, P-, and Sb-doped Si have verified the formation of vacancy-donor defects V-D$_n$, $n > 1$ [25–27] and explained their formation through kinetic processes [28]. PAS has also been used for directly observing the formation of thermal vacancies in highly As- and P-doped Si [29]. In Publ. I, positron annihilation studies in highly As-doped Si are performed to understand why most of the thermally generated vacancies cannot be observed with positrons in As-doped Si compared to P-doped Si [29].

The defects in $Si_{1-x}Ge_x$ resemble closely the ones in pure Si. The dominant defect in both relaxed and strained proton irradiated P-doped $Si_{1-x}Ge_x$ has been shown to be the V-P pair, also called the E center [30, 31]. The electronic levels of the E center in the band gap are shown in Fig. 2.2. The E center in Si has a well-known acceptor level at $E_C - 0.45$ eV [32–34] and recently also a donor level has been found at 0.27 eV above the valence band [21]. In Ge, two acceptor levels have been reported [35] making the E center in Ge a more effective trap for conduction electrons. Due to the increased interest in using $Si_{1-x}Ge_x$ in semiconductor technology, the E center has become the focus of numerous studies in $Si_{1-x}Ge_x$ [30, 31, 36–38]. However, the properties and the formation of this defect are still not fully understood.

Monakhov *et al.* have performed deep level transient spectroscopy studies in n-type strained proton irradiated $Si_{1-x}Ge_x$ samples and report on defect characteristic electronic levels [36, 37]. Kringhøj *et al.* have shown that the distance of the E center acceptor level to the conduction band edge is independent of the Ge content in relaxed $Si_{1-x}Ge_x$ [38]. In previous positron annihilation studies, the E center in $Si_{1-x}Ge_x$ has been shown not to have

any preference for Si or Ge atoms after proton irradiation [31]. However, annealing strained $Si_{1-x}Ge_x$ layers increases the number of Ge atoms around the E center and the subsequently formed V-P-Ge complex is by 0.1–0.2 eV more stable than the simple V-P pair [30]. In Publ. II, the effect of the extra Ge atoms around the E center on the electronic properties of the defect is studied.

2.2.2 Energetics of vacancy defects

Point defects are always present in real crystals since their presence can lower the overall free energy, even though it increases the entropy. Intrinsic defects, such as vacancies and interstitials, all have an equilibrium concentration that is determined by basic thermodynamics.

The room temperature equilibrium concentration of thermal vacancies in Si is low. However, greater concentrations of thermal vacancies form during processes at high temperatures. Although these vacancies are originally mobile (indeed, the processes at high temperature are often used to dissociate defect complexes and remove vacancies) some thermal vacancies can form stable complexes with impurity atoms during the cooling down. Thermal vacancies mediate diffusion of impurity atoms causing the formation of electrically passive defect complexes.

The equilibrium concentration of thermal vacancies in an impurity free material at a temperature T is determined by

$$c_V = e^{-G_f/k_B T}, \tag{2.6}$$

where k_B is the Boltzmann constant and G_f the Gibbs free energy of the vacancy depending on the formation enthalpy H_f and the formation entropy S_f as

$$G_f = H_f - TS_f. \tag{2.7}$$

In the presence of impurities, the vacancy formation next to an impurity atom can reduce the formation energy by the amount of the binding energy between the vacancy and the impurity atom. This must be taken into account in the case of vacancy-impurity defects.

Measurements carried out in P-doped Si show an increase in positron lifetime that is due to thermal vacancies diffusing from the surface (where they

form) into the bulk [29]. However, this effect is greatly reduced in heavily As-doped Si. In fact, as explained above on the basis of Publ. I, most of the thermally generated vacancies cannot be observed in positron annihilation measurements [39].

2.3 Diffusion

Although dopant diffusion can occur by direct-exchange, where the neighboring atoms simultaneously switch positions, the process is very slow compared to indirect diffusion mediated by lattice defects, such as vacancies and interstitials. In vacancy mediated diffusion, a dopant atom jumps to a neighboring empty lattice site. If there is an attractive interaction between the vacancy and the dopant atom, the vacancy and the dopant atom can diffuse as a pair through the lattice. In the case of interstitial mediated diffusion, the interstitial atom kicks the dopant atom from the lattice site into the interstitial position. Afterwards the dopant atom may diffuse via interstitial positions finally settling to a new lattice site by moving a lattice atom to an interstitial position [15, 40]. An interstitial atom and a dopant atom may also diffuse as a pair through the lattice [6, 41, 42].

Diffusion depends strongly on temperature, dopant concentration and impurity atoms. The different mechanisms are a result of the different sizes of the dopant atomic species. In weakly P-doped Si, P diffuses almost totally by interstitial mechanism, whereas in weakly As-doped Si both vacancies and interstitials play a role. Sb diffusion in weakly Sb-doped Si, however, is almost completely vacancy mediated [43, 44]. A well-known problem in B-implantation is the formation of Si interstitials that enhance B diffusion. With time and annealing the interstitials disappear and the B diffusion saturates. This enhanced diffusion is called transient enhanced diffusion (TED) [6].

In general, when the temperature increases, the diffusion gets stronger. In highly n-type Si, the vacancy-donor pairs (V-D) become mobile around 450 K. Some of the V-D defects diffuse to the surface but others form V-D_2 defects, where the vacancy is surrounded by two donor atoms. At even higher temperatures (650–700 K for As and P [28]), these V-D_2 defects form V-D_3 complexes. However, in weakly doped materials kinetic processes limit

the formation of vacancy-impurity clusters [28].

In Publ. I, phenomenon in which thermal vacancies form at the surface of the sample and diffuse into the bulk is studied. The surface concentration is approximated with the thermal equilibrium concentration from Eq. (2.6). Hence, we have a one-dimensional problem and can write the diffusion equation as

$$\frac{\partial c}{\partial t} = \frac{\partial}{\partial x}\left(D\frac{\partial c}{\partial x}\right), \tag{2.8}$$

where c is the concentration of diffusing particles and D the diffusion constant [13]. The diffusion constant is determined by the Arrhenius relation:

$$D = D_0 \exp(-\mathcal{E}_D/k_B T), \tag{2.9}$$

where the activation energy $\mathcal{E}_D$ is the sum of the vacancy formation and migration enthalpies:

$$\mathcal{E}_D = H_f + H_m \tag{2.10}$$

and the prefactor

$$D_0 = \frac{1}{4} f_c a^2 \nu_A \exp[(S_f + S_m)/k_B]. \tag{2.11}$$

Here, a geometric factor $\frac{1}{4}$ takes into account the four directions in space toward which a vacancy can jump, f_c describes the correlation between the subsequent jumps of the atoms, a is the lattice constant, ν_A the jump attempt frequency of the atoms and S_m the migration entropy. For the diamond lattice, $f_c = 1/2$ [45]. The jump attempt frequency can be approximated as the Debye frequency 10^{13} s^{-1}.

2.4 Semiconductor processing and defects

Making semiconductor devices is often balancing between doping and introducing defects that cancel the effect of the dopant atoms. Some defects form already during growth at high temperatures. A well-known problem is that common process stages such as ion-implantation and oxidizing generate point defects such as vacancies and interstitials that could lead to the formation of electrically inactive complexes. Defects can often be removed by annealing the samples at high temperatures, where the defect complexes

dissociate and the defects turn mobile. However, annealing also causes diffusion of dopant atoms, which is undesirable when trying to achieve very thin dopant regions and high dopant concentrations.

Defects can also be introduced deliberately by ion-implantation or irradiation. Irradiation offers possibilities for studying the generation and annealing of simple vacancy defects, as in Publ. III, where neutron irradiated germanium is studied. Especially, very few irradiation induced defects have been identified and studied in Ge, hence gaining knowledge on the formation, migration, and annealing properties of vacancy defects is very important. The low formation energies of vacancy defects in germanium make them suitable agents for self-diffusion and diffusion of impurities [46] and can cause efficient deactivation of donors by the formation of vacancy-donor defects. Theoretical calculations have suggested the presence of divacancies at room temperature [47] and the divacancy has been suggested to have electronic levels in the upper half of the band gap at $E_c - 0.29$ eV [35, 48, 49]. However, there is still controversy whether the divacancy is stable at room temperature due to the lack of direct experimental evidence. Positron lifetime spectroscopy is used in Publ. III for studying the thermal stability, clustering, and annealing of divacancies in neutron irradiated n-type Ge.

Boron-implantation is the most common technique to selectively produce shallow p-doped regions in Si. Smaller and more effective electronic components demand higher and higher dopant densities and reduced junction depths. The problem with ion-implantation is that it produces high concentrations of defects such as self-interstitials and vacancies that increase the dopant diffusion and cause electrically inactive defect complexes. In the presence of self-interstitials boron interacts with them and undergoes transient-enhanced diffusion [6, 50]. The formation of boron-interstitial complexes (BICs) leads to electrical deactivation [50–53]. So far, no suitable technique for commercial use has been found to control B-diffusion and prevent the formation of BICs.

He-implantation is studied in Publ. IV as a means to control B diffusion in crystalline Si. He-implantation has been found to suppress interstitials in both crystalline and pre-amorphized Si [54–57]. By implanting a large dose of He into the sample, a high amount of vacancies is formed at the projected range R_p. During subsequent annealing, these voids can be turned into empty voids [58, 59] that act as sinks for the self-interstitials [60].

The drawback of the method is that the voids can also hinder the performance of the device by introducing deep levels into the band gap which act as recombination centers for carriers [61]. The newly discovered layer of small "nanovoids" at approximately $R_p/2$ has created new interest in the He-implantation technique. These nanovoids have been suggested to cause a significant reduction in B diffusion in the He-implanted samples [55]. The detrimental effect of the deep void layer can be avoided, since the B dopant atoms never approach the R_p of He. Positron annihilation studies of self-implanted and He-implanted Si have also confirmed the existence of vacancy clusters, but systematic studies on the formation kinetics and the dimension of the nanovoids is yet to be carried out.

Excimer laser annealing (ELA) is a tool for annealing implantation damage in Si. In the ELA process, the damaged region in the sample is melted and the subsequent recrystallization removes the defects caused by the implantation. The treatment has obtained a renewed interest, since it enables very shallow and abrupt dopant profiles that could be applied to sub-70 nm technology.

Regardless of the implantation parameters and ELA conditions, a build-up in the B concentration has been observed at the maximum melting depth after multiple pulses of ELA. This pile-up increases with the number of ELA pulses. As a possible explanation, a gradual build-up of vacancies has been suggested [62]. In Publ. V, positron annihilation spectroscopy is used for explaining the observed gradual build-up in the B concentration at the maximum melt depth after multiple pulses of excimer laser annealing.

2.5 Semiconductor defect characterization methods

In this work, positron annihilation spectroscopy is used to study properties of vacancy-type defects. The strength of positron annihilation measurements is the contactless nondestructive depth-dependent identification of defects. The detectable concentration range from 10^{16} cm^{-3} to 10^{19} cm^{-3} is ideal for technological purposes since the range corresponds to the typical dopant densities in semiconductors. The measurements can also be done

at various temperatures and ambient conditions. In fact, the method is not even restricted to semiconductors and metals, but even polymers and liquids can be studied. The drawback of positron spectroscopy is that it requires elaborate equipment and is sensitive only to vacancy-type defects. The positron measurements are also time-consuming, which makes them unsuitable to be used for process monitoring. A more detailed description of PAS is presented in Chapter 3.

Deep level transient spectroscopy (DLTS) is the most common method to observe deep levels in the band gap that are associated with point defects such as vacancies, interstitials or defect complexes [63]. DLTS is applied to a *p*-*n* junction or a Schottky barrier diode that can be fabricated simply by the deposition of a metal film at room temperature over the studied semiconductor material [64]. Also real device structures can be studied [65]. DLTS probes the space-charge region in a Schottky barrier or *p*-*n* junction diode where carrier traps affect the depletion capacitance. DLTS allows the determination of the position of the defect level in the band gap, defect concentration, and thermal emission properties of the defect. Furthermore, the activation energy, concentration profile, and carrier capture cross sections can be measured [64]. Trap densities of the order of 10^{-5} to 10^{-4} times the dopant density can be detected [63]. The drawback of DLTS is that the exact identification of the defects can be impossible [63]. However, comparison to other experimental spectroscopies such as electron paramagnetic resonance (EPR) or positron annihilation spectroscopy helps in identification of the defects.

EPR is a well-established for studying defects in semiconductors [66]. The magnetic resonance spectra contain detailed information on the symmetry and the electronic and lattice structure of the defects. Only paramagnetic defects can be observed, which means that the defects with an even number of electrons are usually undetectable. However, the electrically active defects often have at least one charge state involving an odd number of electrons with a net spin moment that causes paramagnetism [67]. In EPR measurement, Zeeman-split energy levels are detected by causing magnetic-dipole transitions between the levels by applying an alternating magnetic field perpendicular to the steady field. Resonant absorption of microwave frequency photons is observed when the photon energy corresponds to the energy separation between the Zeeman-split levels [13]. EPR measurements have a very good sensitivity and atomic concentrations as low as 10^{-9} can

be detected. Famous examples of the usefulness of EPR are the studies of the intrinsic defects in Si by Watkins [12, 68].

Hall-effect measurement is one of the simplest methods that allows the determination of the carrier density, resistivity, mobility, and carrier type. Spreading resistance profiling (SRP) is a more complicated tool that allows the measurement of the resistance as a function of depth but requires complex sample preparation [63]. These methods cannot be used for defect identification but offer valuable information on the important properties of the semiconductor materials that can be used together with other methods such as PAS or DLTS to gain an overall picture of defect behavior in semiconductor materials.

Secondary ion mass spectroscopy (SIMS) is a destructive method, in which the sample material is removed by sputtering and analyzed by a mass analyzer. It allows quantitative depth profiling of the sample used *e.g.* in determining dopant distribution and the presence of impurities [63]. Dopant densities as low as 10^{15} cm^{-3} can be detected [63]. Vacancies cannot be observed with SIMS, but it can used to reveal diffusion profiles and dopant accumulation that can be affected by vacancies.

Chapter 3

Positron annihilation spectroscopy

Positron annihilation spectroscopy is a powerful method for studying vacancy type defects in materials. It gives information not only on the vacancy size but also on the concentration, charge state, and the chemical surroundings of the vacancy. Positron annihilation spectroscopy is based on the fact that the positron is the antiparticle of the electron and thus will annihilate with an electron when introduced into matter. In a typical annihilation event, two 511 keV gamma photons are emitted into almost opposite directions. In matter, positrons can get trapped into defects of open volume, *e.g.* vacancies. In a vacancy, the electron density is lower causing a detectable increase in the positron lifetime. In addition, information on chemical surroundings of vacancy defects can be obtained by measuring the Doppler-shift of the 511 keV annihilation line.

3.1 Positrons in solids

Positrons are easily obtained as a product of radioactive β^+-decay processes. A practical positron source is ^{22}Na which emits a positron as it decays into ^{22}Ne with the half life of 2.6 a. Simultaneously with the positron, a

1.27 MeV gamma photon is emitted making it possible to detect the birth of the positron.

In a solid, the positron thermalizes rapidly and then diffuses for a few hundred picoseconds. Before annihilating with an electron, the thermalized positron may get trapped into negative or neutral vacancy defects. Due to the reduced electron density in the vacancy, the positron lifetime increases from the bulk lifetime (*i.e.* the lifetime in the perfect lattice). The lifetime can be measured as the time difference between the 1.27 MeV photon and the 511 keV annihilation photon. The positron lifetime distribution can be used to identify vacancy-type defects and to give information on their concentration.

Momentum is conserved in the annihilation, *i.e.* the momentum of the annihilating electron-positron pair is transferred to the two annihilation photons. The momentum of the thermalized positron is small, so that it is the electron momentum which causes a Doppler-shift in the 511 keV annihilation line. The presence of a vacancy affects the local electron momentum distribution. The trapping of positrons at vacancies leads to a narrower Doppler-broadened momentum distribution of annihilating electron-positron pairs compared to free positron annihilation in the lattice. The high-momentum part of the momentum distribution is caused almost entirely by annihilations with the core electrons of the surrounding atoms. Thus, the high momentum distribution can be used to obtain information on the chemical surroundings of the vacancy, *e.g.* to distinguish between vacancies in different sublattices.

Thorough reviews of the method and the theory of positron in solids can be found in Refs. [7–10].

3.2 Positron lifetime spectroscopy

In a positron lifetime setup, the time difference between the 1.27 MeV photon (positron birth signal) and one of the 511 keV annihilation photons is measured. Two examples of typical positron lifetime spectra are presented in Fig. 3.1. The spectrum $n(t) = \sum_i I_i \exp(-t/\tau_i)$ is analyzed as a sum of exponentially decaying components convoluted with the Gaussian resolution

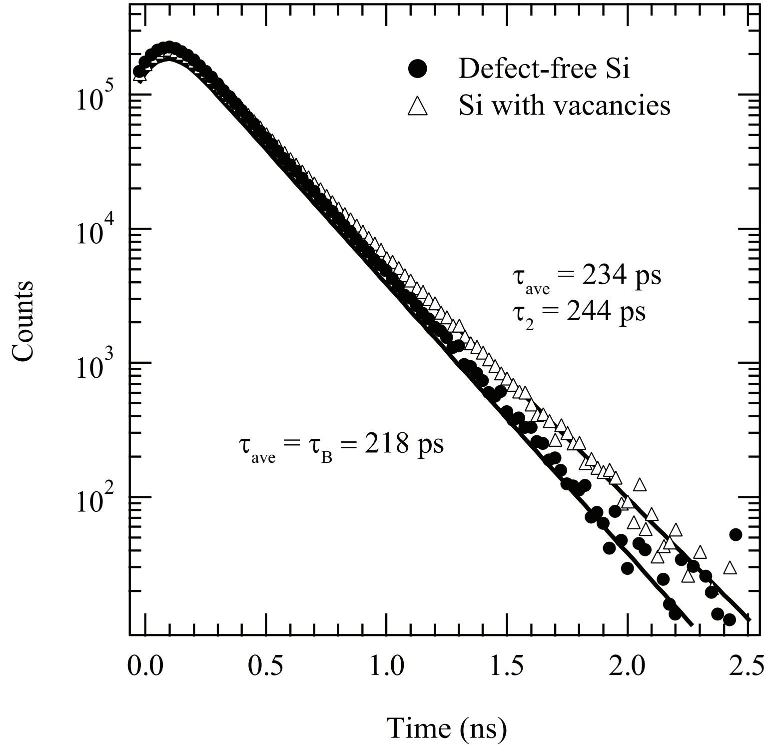

Figure 3.1. *Positron lifetime spectrum in defect-free bulk (blue dots) and in the presence of vacancy defects (red triangles). The lines are fits to the experimental data.*

function of the spectrometer. The indices i correspond to the different lifetime components in the spectrum with individual lifetimes τ_i and intensities I_i.

The average positron lifetime, when N lifetime components can be separated from the lifetime spectrum, is

$$\tau_{ave} = \sum_{i=1}^{N} I_i \tau_i. \tag{3.1}$$

It coincides with the center of mass of the lifetime spectrum and is insensitive to the decomposition. An increase in the average lifetime above the bulk lifetime τ_B (*e.g.* 218 ps in Si) is a clear indication of vacancies being present in the material [7]. Changes even as low as 1 ps can be reliably measured. The concentration of vacancies c_D can be determined from the

average positron lifetime using the conventional positron trapping model. The trapping rate κ of positrons to vacancies is proportional to the defect concentration c_D:

$$\kappa = \mu_D c_D, \tag{3.2}$$

where μ_D is the trapping coefficient, about 1–2$\times10^{15}$ s^{-1} [9].

Each positron state j has a characteristic lifetime $\tau_j = 1/\lambda_j$, where λ_j is the corresponding positron annihilation rate. In the case of single defect type with a specific lifetime τ_D and with no positrons escaping from the defects, the longer positron lifetime component $\tau_2 = \tau_D$ gives directly the defect lifetime, and the shorter lifetime component is the modified bulk lifetime $\tau_1 = (\tau_B^{-1} + \kappa)^{-1}$. The trapping rate derived from the kinetic trapping model is [8]

$$\kappa = \frac{\tau_{ave} - \tau_B}{\tau_D - \tau_{ave}} \lambda_B. \tag{3.3}$$

The lifetime components change if the positron binding energy to the trap is so small that the positrons have a probability to escape (see Publ. I). In the case of one defect type and detrapping, the lifetime components τ_1 and τ_2 depend on the trapping parameters as [8]

$$\begin{aligned} \frac{1}{\tau_{1,2}} &= \frac{1}{2}\{\tau_B^{-1} + \tau_D^{-1} + \kappa + \delta \\ &\pm [(\tau_B^{-1} + \kappa - \tau_D^{-1} - \delta)^2 + 4\kappa\delta)]^{\frac{1}{2}}\}. \end{aligned} \tag{3.4}$$

Thus, the second lifetime component τ_2 depends on κ and δ. The escape rate δ at temperature T is given by [69]

$$\delta = \mu_D \left(\frac{2\pi m^* k_B T}{h^2} \right) \exp\left(-\frac{E_b}{k_B T} \right), \tag{3.5}$$

where E_b is the binding energy of the positron to the trap and m^* is the effective mass of the positron ($m^* \approx m_0$, where m_0 is the electron rest mass). The intensities of the lifetime components in Eq. (3.1) are given by [8]

$$I_1 = \frac{\lambda_B - \lambda_2}{\lambda_1 - \lambda_2} = \frac{\tau_1(\tau_2 - \tau_B)}{\tau_B(\tau_2 - \tau_1)}, \tag{3.6}$$

$$I_2 = \frac{\lambda_1 - \lambda_B}{\lambda_1 - \lambda_2} = \frac{\tau_2(\tau_B - \tau_1)}{\tau_B(\tau_2 - \tau_1)}. \tag{3.7}$$

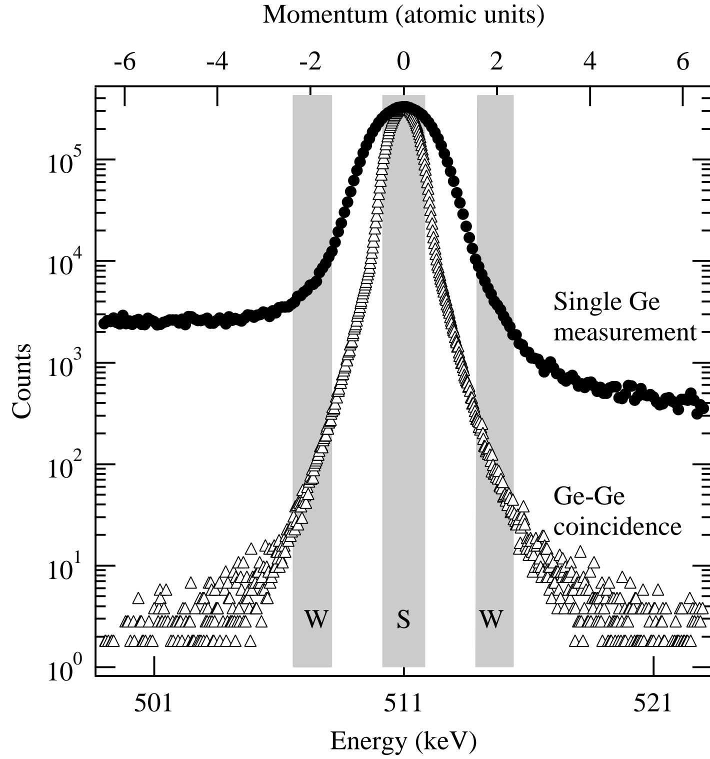

Figure 3.2. *Comparison between single-detector and coincidence modes. The energy windows for the line-shape parameters S and W are also shown.*

3.3 Doppler-broadening measurement

In the Doppler-broadening measurement, the exact energy of the annihilation photons is detected. The electron momentum distribution results in a Doppler broadened energy spectrum, an example of which is presented in Fig. 3.2. Since the detector resolution (1.3 keV at 511 keV) is of the same order of magnitude as the Doppler-broadening, the Doppler spectra are conventionally characterized with the annihilation parameters S and W. The S parameter describes the fraction of positrons annihilating with low momentum electrons, with approximately $|p| < 0.4$ a.u. ($|E_\gamma - 511\text{ keV}| < 0.75$ keV), while W is the fraction annihilating with electrons corresponding to the high momentum "wings" of the 511 keV peak, with approximately 1.6 a.u. $< |p| <$ 2.4 a.u. (2.9 keV $< |E_\gamma - 511\text{ keV}| <$ 4.4 keV).

In a vacancy, the positron has usually a higher probability of annihilating with low momentum electrons and correspondingly a smaller probability of annihilating with electrons of higher momenta. Thus, the vacancy is often detected as an increase in the S parameter and a decrease in the W parameter. However, the annihilation parameters are also sensitive to the chemical environment of the vacancy which complicates the interpretation.

The trapping rate to a vacancy can be estimated from the annihilation parameters in a similar way as in positron lifetime spectroscopy

$$\kappa = \frac{S - S_B}{S_D - S}\lambda_B = \frac{W - W_B}{W_D - W}\lambda_B, \tag{3.8}$$

where the indices D and B correspond to the annihilation parameter values at the defect and in a defect-free bulk, respectively.

The background of the Doppler spectra can be reduced by using two Ge detectors and detecting both annihilation photons in a coincidence setup. This improves the peak to background ratio up to a factor of $\sim 10^6$ (see Fig. 3.2) and allows an accurate measurement of the momentum distribution of the annihilating electrons at high momentum values [70]. The annihilation events are collected in a two-dimensional matrix. The conservation of energy gives $E_1 + E_2 = 2m_0c^2 - E_b$, where E_b is the binding energy of the electron and positron in a solid, so the annihilation events are on the diagonal of the two-dimensional spectrum. Due to the finite resolution of the system, only counts where the sum of the photon energies is within 2 keV to $2m_0c^2$ are accepted to the final 1D spectrum. This improves the resolution of the measurement system by a factor of $\sim\sqrt{2}$. A resolution function of the measurement system can be easily obtained from the other diagonal $E_1 - E_2 = constant$, making it possible to directly compare experimental data to theoretical calculations [71].

3.4 Measurement setups

Positron annihilation measurement setups can be divided into fast and slow positron measurement setups depending on whether positrons are slowed down in order to form a monoenergetic beam or not. Fast positrons are easily available and do not require complicated equipment, but are only

suitable for measuring bulk samples. Slow positron beams are needed for measuring thin layers, typically a few microns thick.

3.4.1 Measurements using fast positrons

Typically in fast positron measurements, two identical sample pieces are used and the positron source is placed between the samples. The stopping profile of positrons from the β^+ radiation is exponential. For the ^{22}Na source, the maximum energy of the positrons is $E_{max} = 0.54$ MeV. The corresponding mean stopping depth of the positrons is, for example, in Si 110 μm. Thus, the fast positrons are best suited for probing homogenous bulk samples with a thickness of several hundreds of micrometers.

The positron lifetime spectrometer has two detectors consisting of a fast scintillator coupled to a photomultiplier tube. Traditionally in an analog setup, constant fraction discriminators are used for obtaining the timing pulses that are in turn fed into a time-to-amplitude converter. The pulses are then collected into a lifetime spectrum by a multichannel analyzer.

A typical positron lifetime (or Doppler-broadening) spectrum has 1–2 million counts. The annihilations of positrons in the source material, in the Al- or Ni-foil covering the source and as positronium are determined by using a reference sample and subtracted from the lifetime spectra before the decomposition of lifetime spectra.

The Doppler-broadening of the annihilation radiation can be measured simultaneously with the positron lifetime by using a high purity Ge detector. The sample temperature during the measurement can be controlled with resistive heating and either liquid-nitrogen or closed-cycle He cooling.

3.4.2 Slow positron beam

When a studied sample or layer in a sample is considerably thinner than a few hundreds of micrometers required for the fast positron measurements, slow positrons are needed. In a slow positron beam, a thin tungsten foil with a negative positron work function is used for moderating positrons af-

ter they are emitted from the source. Unmoderated positrons are discarded and moderated positrons are accelerated in an electric field in order to create a tunable-energy (0.5–38 keV) beam of slow positrons. In this work, two Ge detectors were used to collect the radiation from the annihilation events. In some measurements the detectors were used in coincidence mode as described in Sec. 3.3. In other measurements, the spectra from the two detectors were summed after scaling the spectra with the single detector resolutions, and conventional S and W parameters were used to describe the shape of the Doppler-broadened annihilation line [7]. The sample temperature during measurements could be controlled by a closed-cycle He cryostat and with resistive heating.

Chapter 4

Vacancy-donor complexes related to n-type doping in silicon and silicon-germanium

We show that the difficulties in observing thermally generated vacancies in highly As-doped Si are due to escape of positrons from V-As_3 defect complexes in Publ. I. The positron Doppler-broadening techniques are used for obtaining evidence on a second acceptor state of the V-P pair in $Si_{1-x}Ge_x$ in Publ. II.

4.1 Positron trapping kinetics in highly As-doped silicon

Positron binding energies to vacancy-type defects in semiconductors are typically of the order of ∼0.5 eV [72]. Thus, the traps are so deep that positrons cannot escape by thermal excitations before the sample melts, and positrons annihilate as trapped at the defect. Defects with a small positron binding energy, from which the positron can detrap with phonon-assistance, are called as shallow traps. Typical examples of shallow traps

include dislocation lines in metals and Rydberg states around negative ions in semiconductors. These shallow traps capture positrons at low temperatures. In the case of vacancy-type defects the binding energies are larger but in some cases low enough for positrons to escape above room temperature.

4.1.1 Thermal generation of vacancies

In order to directly observe the formation of thermal vacancies, we measured the average positron lifetime in Si samples with strong As-doping as a function of measurement time above room temperature [39]. Our samples were Czochralski-grown Si(111) bulk crystals doped with As to a concentration of 1×10^{20} cm^{-3}. The as-grown sample contained a small concentration of $\sim10^{17}$ cm^{-3} of native V-As$_3$ defects [73]. Before the measurements, the average positron lifetime in the as-grown sample was 226 ps, while the lifetime in a defect-free lattice is 218 ps.

When the positron lifetime was measured in the as-grown sample at 700 K, it had decreased to 220 ps from the value at room temperature. We performed isothermal annealings at 700, 750 and 800 K and measured the average positron lifetime *in situ* at the annealing temperatures. The results are shown in Fig. 4.1.

The positron lifetime starts to increase already at 700 K. During the 180 h annealing at 750 K, the average positron lifetime increases to a value of 224 ps. During the annealing at 800 K the average lifetime shows signs of saturation to 225 ps. After the long annealing at 800 K and cooling down, the positron lifetime was measured at room temperature. Interestingly, the room temperature lifetime had increased to a value of 234 ps. This lifetime is considerably longer than the one measured during the annealing at 800 K and suggests that only a small number of vacancies trap positrons at high temperatures.

The increase in the average positron lifetime during high-temperature annealing has previously been observed in highly P-doped Si [29] and is due to thermal vacancies diffusing from the surface, where they form, into the bulk. However from Fig. 4.1, one can see that the average positron lifetime in As-doped Si is smaller at 700 K than at room temperature suggesting that only a small fraction ($\sim$ 15 %) of vacancies can be observed with posi-

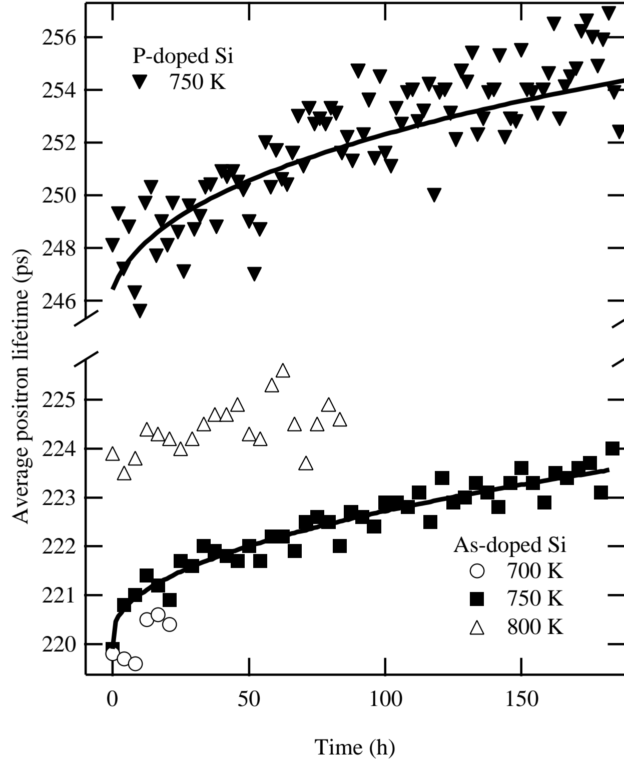

Figure 4.1. *Average positron lifetime in the as-grown Si([As]=*10^{20} cm^{-3}*) sample as a function of measurement time for different measurement temperatures. For comparison, the data from the Si([P]=*10^{20} cm^{-3}*) sample from Ref. [29] is also included. The solid curves are from the solution of the diffusion equation.*

tron measurements at temperatures above 700 K. Despite the difficulties in observing thermal vacancies at high temperatures, the resulting increase in the room temperature positron lifetime indicates an increase in the vacancy concentration from 4×10^{17} cm^{-3} in the as-grown sample to 1×10^{18} cm^{-3}. This shows that thermal vacancies form abundantly and form stable vacancy impurity complexes during cooling down.

4.1.2 Positron trapping at the V-As_3 complex in silicon

To find out the reason for the difficulties in observing vacancies with positrons at high temperatures and to explain the increase in the positron room temperature lifetime as a result of the annealings, we measured the positron lifetime in the temperature range from 180 to 700 K. In addition to the as-grown sample and the sample annealed at 800 K, we measured two samples, which had previously been annealed at 900 and 920 K until thermal equilibrium was achieved and then cooled down to room temperature, as reported in Ref. [29]. The results are shown in Fig. 4.2. Due to the different vacancy concentrations depending on the thermal histories of the different samples, the room temperature values differ from each other. The average positron lifetime behaves similarly in all samples. The lifetime remains constant until 400 K where it starts to decrease. The decrease continues until 700 K where it shows signs of saturation in the two samples with the lowest vacancy concentrations (*i.e.* the as-grown sample and the sample annealed at 800 K).

We decomposed the lifetime spectrum into two components and noted that the longer lifetime component τ_2 decreases in the two samples with smaller vacancy concentrations. This can be explained by positrons detrapping from the vacancies at high temperatures. The longer lifetime component does not decrease in the two other samples. In the sample annealed at 900 K, the longer lifetime component is constant, whereas in the other sample τ_2 even increases.

The Doppler-broadening of the annihilation radiation was measured simultaneously with the positron lifetime and the S and W parameters as a function of temperature are presented in Fig. 4.3. The parameters have been scaled to the bulk values of $S_B = 0.4296$ and $W_B = 0.04229$. At room temperature, the S parameter is lower and the W parameter is higher than the bulk value. This is due to the ten $3d$ electrons of each of the three As atoms decorating the vacancy. These three atoms increase the relative intensity of the core electron momentum distribution [26, 73]. When the temperature is increased from room temperature, the S and W parameters approach the bulk values. Thus, the signal from the As-atoms decreases.

We used the kinetic trapping model presented in section 3.2 to fit the av-

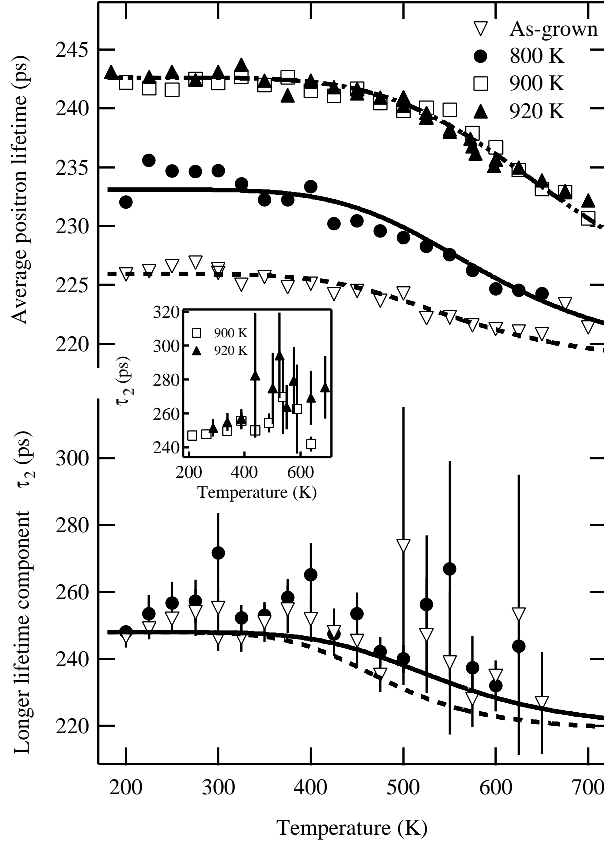

Figure 4.2. *The average positron lifetime and the longer lifetime component as a function of measurement temperature. The lines have been fitted to the average lifetime data using the kinetic trapping model and the lines among the longer lifetime component data have been calculated from those fits. The inset shows the longer lifetime component in the two samples with the highest defect concentration.*

erage lifetime data in Fig. 4.2. The fit gives a positron binding energy of 0.27(3) eV to the trap and a defect concentrations of 4×10^{17} cm^{-3}, 1×10^{18} cm^{-3}, 5×10^{18} cm^{-3} and 5×10^{18} cm^{-3}, for the untreated sample, and the samples annealed at 800, 900 and 920 K, respectively. From the fits to the lifetime data, the corresponding S and W parameter curves were calculated. The calculated curves presented in 4.3 show that the Doppler results are in good agreement with the lifetime data.

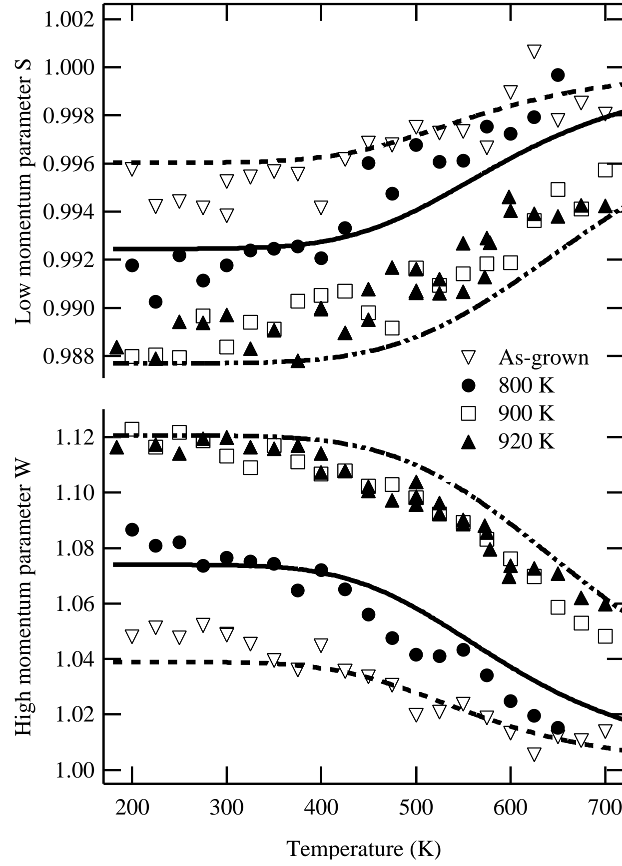

Figure 4.3. *Low momentum Doppler parameter S and the high momentum Doppler parameter W as a function of measurement temperature. The parameters have been scaled to the bulk values. The lines are calculated from the fits to the average lifetime data.*

In the two samples that had been annealed at 900 and 920 K, and which thus had the highest vacancy concentration ($\sim 10^{19}$ cm^{-3}), the longer lifetime component does not show the decrease associated with detrapping. In these samples, the vacancy concentration is approaching the limit where all the As atoms are part of V-As_3 complexes since the dopant concentration is $\sim 10^{20}$ cm^{-3}. A V-As_3 complex is formed from a diffusing V-As_2 complex, when it meets yet another As atom [28]. When the concentration of V-As_3 defects increases, it is more and more likely that a diffusing V-As_2 complex meets a ready-made V-As_3. The result is a defect where a divacancy is

decorated by five As atoms, V_2-As_5.

V-As_3 dominates at room temperature making it impossible to observe V_2-As_5 complexes. As the temperature is increased and positrons escape from the V-As_3 complexes, the trapping into V_2-As_5 becomes visible in the higher lifetime component. The positron lifetime in an undecorated Si divacancy is 290 ps [74], so the characteristic lifetime of V_2-As_5 is likely to be close to that value or slightly smaller due to the As-decoration. The concentration of the divacancy-donor complexes is, however, small, so the overall trapping to vacancies still decreases causing the decrease in the average positron lifetime. In the V_2-As_5 complex, the S parameter is higher and W lower than in V-As_3 and hence the S parameter increases and the W parameter decreases with increasing temperature more rapidly than what could be expected from the lifetime data. The presence of the V_2-As_5 complex has been reported in highly As-doped Si and studies have shown that the concentration of V_2-As_5 increases dramatically during annealings at 800°C [26]. This is consistent with the fact that the effect of V_2-As_5 is seen in the two samples with the highest annealing temperatures and that the strongest effect can be seen in the sample annealed the longest time at the highest temperature.

The results from the As-doped silicon are compared with the ones obtained from P-doped material in Fig. 4.1. It is evident that the increase in positron lifetime is much larger in P-doped silicon. This suggests that the positrons do not escape from the V-P_3 complex at these temperatures. In the As-doped case, the positron detrap from V-As_3 and the vacancies seen at high temperatures are monovacancies decorated with only one or two As atoms or divacancy type defects such as V_2-As_5.

4.2 The E center in silicon-germanium

The $Si_{1-x}Ge_x$ samples studied in Publ. II were grown on Czochralski Si(100) substrates, as in Ref. [31]. Relaxation of the $Si_{1-x}Ge_x$ layer was achieved by using a buffer layer with an increasing Ge content on top of the substrate. Ge content in the epitaxially grown $Si_{1-x}Ge_x$ layers varied between 10 % and 30 % and the layer thickness was $\gtrsim 2$ μm. The samples were of n-type with a P concentration of 10^{18} cm^{-3}. Irradiation with 2 MeV protons with a fluence of 1.6×10^{15} cm^{-2} produced a homogeneous defect distribution and

a V-P defect concentration $\gtrsim 10^{18}$ cm^{-3}. The effect of the irradiation has been shown in Ref. [31].

The samples were annealed isothermally at 250 and 300°C for 114 and 7 h, respectively. Between the annealings, the Doppler parameters S and W were measured. The behavior of the parameters was similar in all annealed samples. The low momentum parameter S decreases as a function of annealing time, while the high momentum parameter W initially increases and then remains constant. The increase in the W parameter value signals increased positron annihilation with high momentum electrons revealing that the average number of Ge atoms around the E center increases during the annealing. The continuing decrease in the S parameter suggests that some of the defects recover during the annealing.

The positron trapping into negatively charged defects is dependent on the measurement temperature, when the concentration of vacancy defects is below the saturation trapping level. After the annealings at 250 and 300°C, we measured the Doppler-broadening as a function of temperature to see whether the concentration of defects had fallen below the saturation level. Figure 4.4 shows the low momentum parameter S as a function of measurement temperature. The parameter values have not been scaled since a simple reference value cannot be used for samples with different Ge contents.

The S parameter increases slightly with decreasing temperature down to 180 K in the annealed $Si_{0.9}Ge_{0.1}$ samples. Thus, the positron trapping is no longer in saturation and some of the defects have recovered. The small increase shows that the remaining defects are in a negative charge state. At approximately 150 K, the S parameter decreases in all measured samples suggesting a decrease in the open volume of the defects. The W parameter remains constant indicating that the chemical surroundings of the positron annihilation site does not change.

To find out the the reason for the observed decrease in the S parameter, coincidence Doppler-broadening measurements were performed both at room temperature and at 100 K in the irradiated $Si_{0.8}Ge_{0.2}$ sample annealed at 250°C. The results in Fig. 4.5 are shown with the data from the untreated and irradiated samples measured at room temperature. The data have been scaled to a p-type Si reference, where no positron trapping to defects has been observed. At low momenta, the coincidence Doppler spectrum in the as-grown sample resembles closely the Si reference due to the similarity of

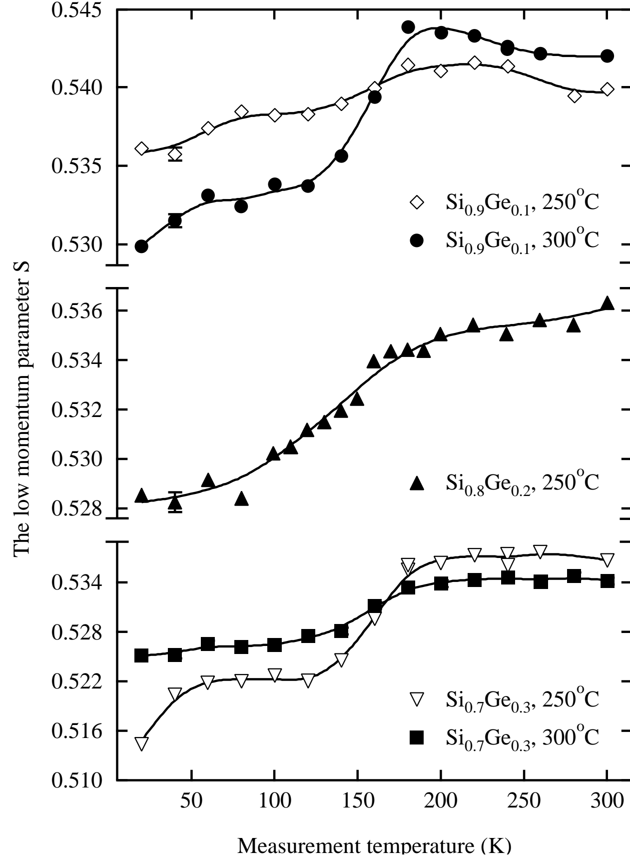

Figure 4.4. *The low momentum parameter S as a function of measurement temperature. The error bars in the $Si_{0.7}Ge_{0.3}$ samples are of the same size as the markers. The solid curves have been drawn to guide the eye.*

the valence electrons in Si and Ge. However, at higher momenta ($p > 1$ a.u.) the $3d$ electrons of Ge increase the intensity relative to the Si reference.

The irradiation induced vacancies increase the intensity of the momentum distribution at low momentum values ($p < 0.4$ a.u.). The reduced intensity at high momentum values is due to the reduced overlap of the positron wave function with core electrons. The peak at approximately 1.4 a.u. has two possible explanations. The first explanation is that the overlap of the positron wave function with the anisotropic electron momentum distribution in the diamond structure is reduced [7, 28]. Another explanation rises from the fact that the momentum of the positron localized at the vacancy is

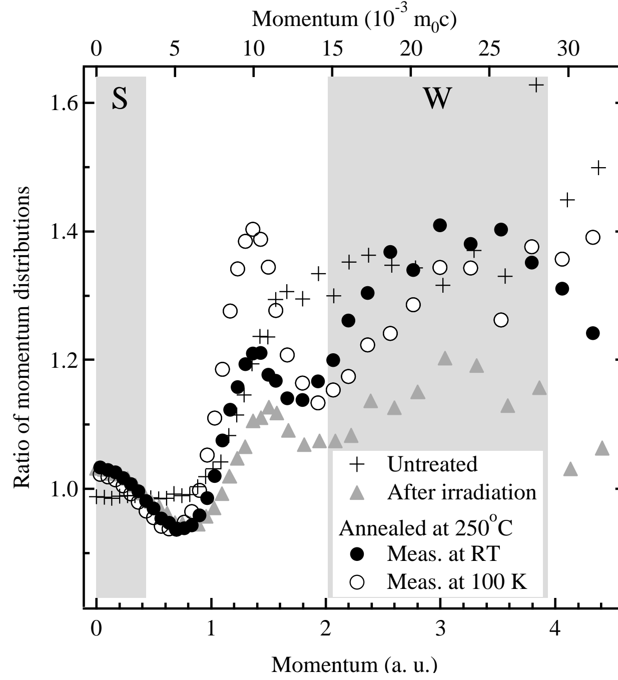

Figure 4.5. *Coincidence Doppler spectra of the $Si_{0.8}Ge_{0.2}$ layers. The data have been scaled to the one measured from a Si reference sample, where no positron trapping is observed. The data from both the untreated sample and the sample after irradiation have been measured at room temperature.*

increased. This increase in the positron momentum causes widening of the resolution function which causes the peak in question [75]. In both cases, however, the peak is enhanced when the positron is better localized at the vacancy.

Annealing at 250°C results in an increase in the intensity of the momentum distribution at high momentum values. This is due to the increased number of Ge atoms around the V-P defect. Interestingly the intensity of the 1.4 a.u. peak is enhanced in the momentum distribution measured at 100 K. This indicates that the positron state is narrower and it is more localized in the vacancy.

We interpret the S parameter decrease with decreasing temperature at 150 K as the inward relaxation of the E center. The fact that the W parameter shows no change in the chemical surroundings of the vacancy

supports this interpretation. Taking also the stronger localization of the positron into the vacancy into account, we claim that the E center goes through a transition to a more negative charge state at 150 K.

S parameter increases with decreasing temperature in the annealed samples with 10 % of Ge and a P concentration of 10^{18} cm^{-3} in the interval of 200–300 K. Thus, the vacancies are clearly in a negative charge state, and the transition (0/-) [36, 38, 76] cannot be the one observed here. In pure Si, the neutral E center relaxes inward when it captures an electron [77], but energy levels above (0/-) have not been observed. However, introducing Ge atoms at high concentration can change the situation, since in Ge [78] and Ge-rich $\mathrm{Si}_{1-x}\mathrm{Ge}_x$ [79] the acceptor level (-/- -) has been shown to exist. Thus, when adding more and more Ge into $\mathrm{Si}_{1-x}\mathrm{Ge}_x$ at some point the (-/- -) level moves into the forbidden gap. Therefore, we interpret that the step occurring in the positron Doppler parameters at 150 K corresponds to the energy level (-/- -) of the E center. This transition was not observed in Ref. [30], where the E center was decorated with one Ge atom only. However, in our samples the V-P pair is surrounded by several Ge atoms. Our result shows that in order for the second acceptor level to be pulled down into the band gap, a local increase in the number of Ge atoms around the E center is enough.

To conclude, the charge transition observed at 150 K corresponds to the energy level (-/- -) of the E center. The decoration of the V-P pair by several Ge atoms pulls down the (-/- -) level into the band gap. This conclusion is supported by the higher annealing temperature compared to Ref. [30], where it was shown that a neighboring Ge atoms stabilizes the E center by 0.1–0.2 eV. Also the preliminary theoretical calculations support this idea [80]. The existence of the second acceptor state makes the E center decorated with several Ge atoms a more effective trap for the conduction electrons than a simple V-P pair.

Chapter 5

Defects in silicon and germanium caused by post-growth processing

In this Chapter, neutron-irradiation and ion-implantation produced damage is studied in germanium and silicon. The effect of neutron-irradiation and annealing of n-type germanium is studied in Publ. III. He-implantation is studied as a means to control B diffusion in crystalline Si in Publ. IV. Finally, the generation of vacancies during eximer laser annealing (ELA) of Si is investigated with positron Doppler-broadening technique in Publ. V.

5.1 Divacancy clustering in neutron-irradiated germanium

Our measured Ge samples were n-type bulk crystals with (110) orientation and a Sb concentration of 1.5×10^{15} cm^{-3}. The samples were irradiated with fast neutrons up to a fluence of approximately 10^{16} cm^{-2} and then annealed at 200, 400 and 500°C for 30 min. Since two identical samples were not available, the measurements were performed by sandwiching the

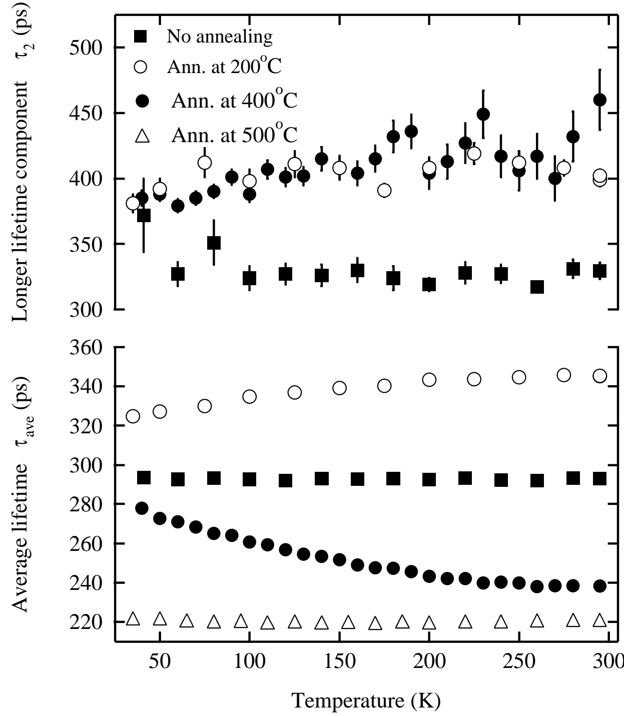

Figure 5.1. *The average positron lifetime τ_{ave} and the higher lifetime component τ_2 as a function of the measurement temperature.*

^{22}Na source between the studied sample and a reference bulk sample with a positron lifetime of $\tau_B = 224$ ps. The annihilations in the reference sample were subtracted from the lifetime spectra along with the common source corrections.

We measured the positron lifetime as a function of measurement temperature ranging from 35 K to 295 K. The results are shown in Fig. 5.1. After the irradiation, before the annealings, the average positron lifetime $\tau_{ave} = 293$ ps is clearly over the bulk lifetime proving that the irradiation produced vacancy defects. A longer lifetime component of 330 ps can be separated from the spectrum that has no observable temperature dependence. The lifetime of 330 ps is close to the calculated value of 316 ps for a Ge divacancy [81] and clearly above the calculated value of 265 ps [81] and suggested experimental values of 290, 292 and 278 ps [82–84] for a monovacancy. Thus, we attribute the lifetime of 330 ps to the neutral Ge divacancy.

Annealing at 200°C resulted in an increase in the average positron lifetime. This suggests that the divacancy defects become mobile and form bigger clusters. This is backed up by the longer lifetime component of 430 ps and the intensity of 68 % at room temperature corresponding to a positron lifetime in a large vacancy cluster of about 10 missing atoms [85–87]. At the same time, however, both the average positron lifetime and the longer lifetime component show a decrease with decreasing temperature. This suggests that some smaller defects, that are in a negative charge state, remain and cause increased trapping of positrons at low temperatures.

The annealing treatment at 400°C results in a decrease in the average positron lifetime signaling that the large vacancy clusters start to anneal. The smaller negative defects are still visible and from the results a lifetime value of 280–320 ps can be estimated. After annealing at 400°C, the negative charge state of the defect is also seen as an increase from 10 % at room temperature to ∼45 % at 40 K in the intensity of the longer lifetime component I_2. The small defect is thus most likely a negatively charged divacancy. Interestingly there are still negatively charged smaller vacancies left after the annealing at 400°C, even though the reported annealing temperature for divacancies is lower [88]. Hence, we can conclude that as the crystal recovers and neutral divacancies agglomerate into larger clusters, the samples gradually become n-type and at least a part of the divacancies turn into a more negative charge state. Calculations by Janke *et al.* [47] indicate that the negatively charged divacancy is more stable than the neutral one. This gives a possible explanation for the persistence of negative divacancies after the 200°C anneal. Finally, annealing at 500°C is enough to remove all observed vacancy defects. From the results of the as-irradiated sample, a concentration of divacancies of the order of 1×10^{17} cm^{-3} can be estimated, so that it is clear that the divacancy is stable at room temperature.

5.2 Vacancy clusters in He-implanted silicon

We used a slow positron beam at room temperature to measure Czochralski grown n-type Si (100) samples implanted with 80 keV He ions (projected range $R_p \approx 600$ nm) at fluences ranging from 5×10^{15} to 8×10^{16} cm^{-2}. We also measured two samples with a He fluence of 3×10^{16} cm^{-2} and implantation energies of 50 and 110 keV. In addition to He-implantation, some

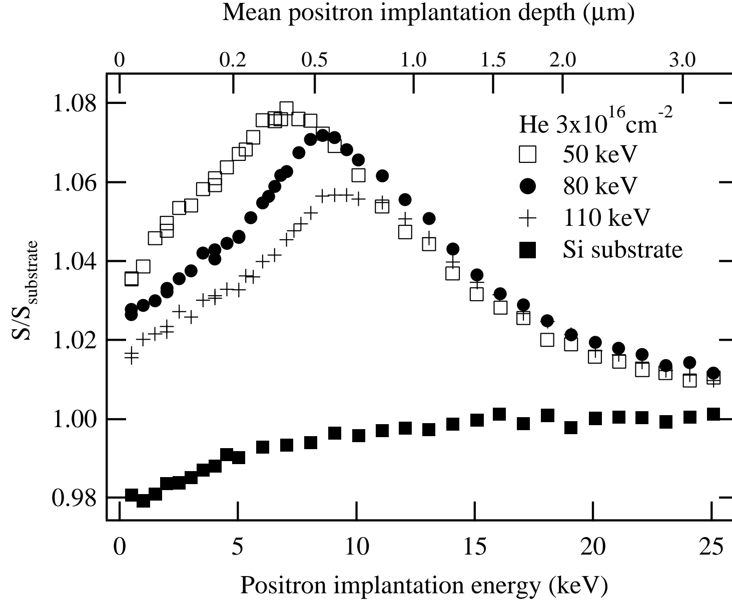

Figure 5.2. *Effect of He implantation energies: The low momentum parameter S in He-implanted and annealed Si samples as a function of the positron implantation energy.*

of the samples were implanted with 12 keV B atoms ($R_p \approx 50$ nm) at 5×10^{14} cm^{-2}. The implantations were carried out at room temperature with a flux of ~1–2 μA/cm^2. Except for three as-implanted samples, all the samples were subjected to annealing for 10 min at 800°C. Prior to the measurements, the native oxide was removed by HF etching.

The effect of He-implantation energy to the S parameter data is shown in Fig. 5.2. The most prominent feature in all data sets is the high peak at R_p of the He atoms corresponding to the positron implantation energies of 6–10 keV. The position of the peak reflects the different projected ranges of the samples. The interesting feature is the shoulder at approximately 3–6 keV corresponding to a positron average stopping depth of ~100–300 nm. The shoulder indicates a change in the positron diffusion length and an annihilation state different from the surface and the end-of-range defects.

Figure 5.3 shows an example of the S parameter data from the samples with a He fluence of 3×10^{16} cm^{-2} and from the annealed sample with a

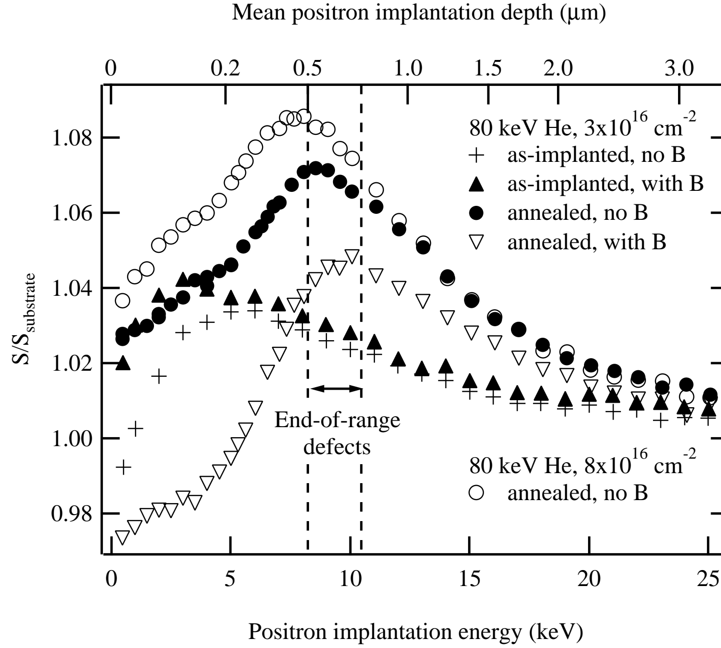

Figure 5.3. *Low momentum parameter S in the He-implanted samples with the implantation fluence of* 3×10^{16} cm^{-2} *and in the annealed sample with a fluence of* 8×10^{16} cm^{-2} *as a function of positron implantation energy.*

fluence of 8×10^{16} cm^{-2}. Both curves from the He-implanted and annealed data show the same two features described earlier. The S parameter value of 1.06 times the Si substrate suggests "nanovoid" defects that are at least slightly larger than divacancies ($S_{V_2} = 1.05 \times S_{\text{bulk}}$ [74]).

The boron-implanted and annealed samples show a different behavior. In these samples the peaks at R_p are smaller than in the samples with only He-implantation meaning that either the defects are smaller in size or that their concentration is lower. The trapping in the nanovoid region at 3–5 keV is different in these samples. The S parameter is close to the Si substrate value suggesting that nanovoids do not trap positrons. This indicates that the nanovoids are filled during the B-implantation. Since the B diffusion length at 800°C for 10 min is only ∼140 nm in the case of interstitial supersaturation, the B atoms do not reach the nanovoid region. Thus, the atoms filling the nanovoids are interstitials created during the B-implantation. These results are in good agreement with previously obtained SIMS results, in

which reduced diffusion of B has been observed at $R_p/2$, and TEM results that suggest the presence of a nanovoid layer [55]. The measurements in the as-implanted samples both with and without B show that the precursors of the nanovoids are already present prior to the annealing. The nanovoids get filled during the annealing at 800°C following B-implantation.

Our results thus explain the mechanism by which the He-implantation creates traps for self-interstitials generated by B-implantation. This leads to the reduction of B diffusion and creates a box-like shape of B-implanted profile making He implantation a useful tool for controlling B distribution in microelectronics applications.

5.3 Vacancy generation in ELA processing of silicon

In Publ. V, we used positron annihilation spectroscopy to study vacancy-type defects in B-doped Si samples after multiple (1–100) excimer laser annealing (ELA) pulses. A Lambda Physic LPX 205 XeCl excimer laser (λ = 308 nm, 28 ns pulse duration, and 6×6 mm^2 spot) was used in the multishot (1–100) regime to irradiate the samples. The thickness of the melted layer was either 50 nm or 150 nm. The laser energy of 1030 mJ/cm^2 was used for thinner samples and 1220 mJ/cm^2 for the thicker ones excluding a sample which was treated with an ELA energy of 1205 mJ/cm^2. Prior to the measurements, the native oxide was removed by HF etching.

Stochastic atomistic simulations in Publ. V suggest trapping of divacancies in the recrystallized region. Continuum phase-field simulations of the multishot process show that between two subsequent pulses, free vacancies recombine with interstitials and at the surface. The subsequent pulse removes residual vacancy clusters residing within the melted region. However, the divacancy profiles extend well beyond the maximum melt depth due to the fast diffusion of vacancies and thus the subsequent laser pulse is unable to remove all the vacancies generated by the previous pulse. The vacancy defects accumulate, pulse by pulse, just beyond the maximum melt depth and finally reach a saturation concentration above 10^{16} cm^{-3}.

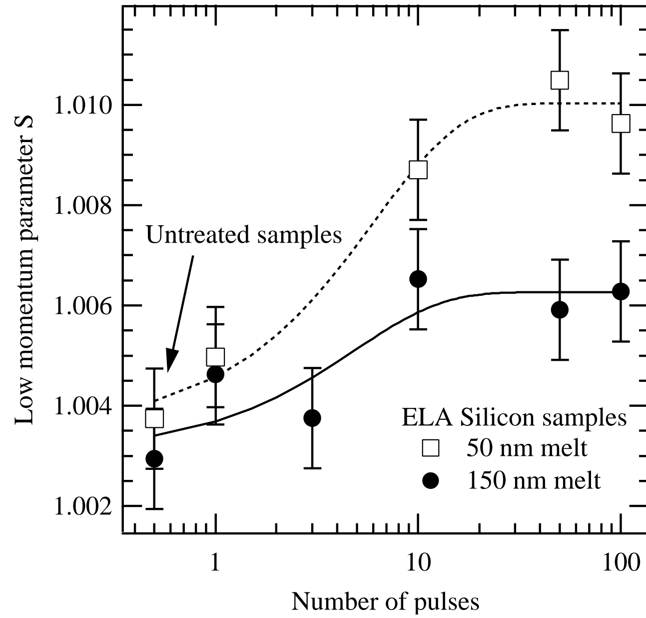

Figure 5.4. *S parameter in the ELA-treated Si samples as a function of the number of laser annealing pulses from Publ. V. The curves have been drawn to guide the eye.*

We used a slow positron beam to measure the Doppler-broadening of the annihilation radiation at room temperature. The results are shown in Fig. 5.4. The S parameter values in the melted near-surface region are above the bulk value of 1, signaling the presence of vacancy defects. The value of the S parameter in the laser-irradiated samples is definitively larger than in the untreated samples. The effect is stronger in the samples with the 50 nm melt depths. Fig. 5.4 shows the S parameter averaged over the melted layer (in the range of 1–2 and 1–4 keV of the positron implantation energy for the samples with 50 nm and 150 nm melt depths, respectively). The S parameter increases with the number of laser pulses until saturation is reached after approximately 10 pulses. This indicates that the total observed open volume increases with the number of pulses. However, the exact identification of the vacancy defects is difficult due to the vicinity of the surface.

Our results confirm the presence of vacancies in the samples. The effect is stronger in the samples with a thickness of 50 nm. The number of vacancies in the samples with both thicknesses increases with the number of ELA

pulses. The observed vacancy defects are present only in the melted layer, with no changes deeper in the material. The positron implantation profile broadens with increasing implantation energy [27]. Hence the weaker effect in the samples with a melt of 150 nm could be caused either by a lower total concentration of vacancy defects in the melted layer or by a peaked concentration profile located at the maximum melt depth as predicted by the calculations. Based on the 1 % increase in the S parameter during the laser annealings, we estimate the vacancy concentration to be in the low range of 10^{16} cm^{-3} in the melted layers, as also predicted by the simulation. Hence the vacancies could be responsible for the B build-up observed in Ref. [89].

Chapter 6

Summary

In this thesis, vacancy-type point defects were studied in group IV semiconductors Si, $Si_{1-x}Ge_x$ and Ge by positron annihilation spectroscopy. These lattice defects form during the growth and processing of the material and they greatly influence the electrical properties of the semiconductor materials by introducing defect levels in the band gap that trap charge carriers. Point defects also cause increased dopant diffusion and clustering. The smaller and smaller transistors require high dopant densities and both shallow and sharp dopant profiles, so the understanding the formation and physical properties such as recovery during thermal annealing of harmful defects is crucial.

In this work, both positron lifetime and Doppler-broadening of the 511 keV annihilation line has been measured to characterize vacancy defects at the atomic level. Firstly, the vacancy-donor complexes were studied in n-type Si and $Si_{1-x}Ge_x$. In Publ. I, we explain why most of the V-As_3 defects cannot be observed during positron measurements at high temperatures by showing that the positrons escape from the defects due to the low binding energy to the V-As_3 defect. The detrapping of positrons from the the V-As_3 complex explains why the increase in the average positron lifetime due to thermal vacancies is smaller in As-doped Si than in P-doped Si at high temperatures, in spite the similarity of the vacancy formation energies in these two materials. In Publ. II, we investigate the effect of the increased number of Ge atoms around the V-P pair in $Si_{1-x}Ge_x$ and show that the

decoration of the V-P pair with several Ge atoms pulls down the second acceptor level (-/--) down to the band-gap. This makes the Ge-decorated V-P pair an especially effective trap for the conduction electrons.

Thermal stability, clustering and annealing of divacancies in Ge is studied in Publ. III. The positron lifetime data shows that the divacancy in Ge is stable well above room temperature. Negative charge state of divacancies is found to stabilize the defects even at 400°C and the divacancy is shown to form bigger clusters before finally annealing at 500°C.

Finally, two methods to control and remove boron-implantation induced damage is studied in Publs. IV and V. Our result from the He-implanted Si confirms that the nanovoid region that forms close to the surface is responsible for diminishing the detrimental effect of B-implantation induced damage. Thus, the He-implantation is shown to be a good tool for producing sharp B profiles. The positron Doppler-broadening experiments from the Si samples subjected to multiple excimer laser pulses, show an accumulation of vacancy defects over subsequent pulses confirming theoretical predictions.

Bibliography

[1] F. Schäffler, Semicond. Sci. Technol. **12**, 1515 (1997).

[2] J. Bardeen and W. H. Brattain, Phys. Rev. **74**, 230 (1948).

[3] S. Verdonckt-Vandebroek, E. F. Crabbe, B. S. Meyerson, D. L. Harame, P. J. Restle, J. M. C. Stork, and J. B. Johnson, IEEE Trans. Electron Devices **41**, 90 (1994).

[4] S. E. Thompson, M. Armstrong, C. Auth, S. Cea, R. Chau, G. Glass, T. Hoffman, J. Klaus, Z. Ma, B. Mcintyre, A. Murthy, B. Obradovic, L. Shifren, S. Sivakumar, S. Tyagi, T. Ghani, K. Mistry, M. Bohr, and Y. El-Mansy, IEEE Electron Device Lett. **25**, 191 (2004).

[5] M. L. Lee, E. A. Fitzgerald, M. T. Bulsara, M. T. Currie, and A. Lochtefeld, J. Appl. Phys. **97**, 011101 (2005).

[6] S. C. Jain, W. Schoenmaker, R. Lindsay, P. A. Stolk, S. Decoutere, M. Willander, and H. E. Maes, J. Appl. Phys. **91**, 8919 (2002).

[7] K. Saarinen, P. Hautojärvi, and C. Corbel, in *Identification of Defects in Semiconductors*, edited by M. Stavola (Academic Press, San Diego, 1998), Vol. 51A, p. 209.

[8] P. Hautojärvi and C. Corbel, in *International School of Physics Enrico Fermi, Course CXXV*, edited by A. Dupasquier (IOS Press, Amsterdam, 1993).

[9] R. Krause-Rehberg and H. S. Leipner, *Positron Annihilation in Semiconductors* (Springer, New York, 1999).

[10] M. J. Puska and R. M. Nieminen, Rev. Mod. Phys. **66**, 841 (1994).

[11] M. Lannoo and J. Bourgoin, *Point Defects in Semiconductors I. Theoretical Aspects* (Springer-Verlag, Berlin Heidelberg, 1981).

[12] J. Bourgoin and M. Lannoo, *Point Defects in Semiconductors II. Experimental Aspects* (Springer-Verlag, Berlin Heidelberg, 1983).

[13] S. Elliot, *The Physics and Chemistry of Solids* (Wiley, Chichester, 1998).

[14] H. Ibach and H. Lüth, *Solid-State Physics. An Introduction to Principles of Materials Science*, 3rd ed. (Springer-Verlag, Berlin Heidelberg, 2003).

[15] P. M. Fahey, P. Griffin, and J. D. Plummer, Rev. Mod. Phys. **61**, 289 (1989).

[16] E. E. Haller, Mater. Sci. Semicond. Process. **9**, 408 (2006).

[17] J. Vanhellemont and E. Simoen, J. Electrochem. Soc. **154**, H572 (2007).

[18] D. J. Paul, Adv. Mater. **11**, 191 (1999).

[19] T. E. Whall and H. C. Parker, J. Mater. Sci. - Mater. Electron. **6**, 249 (1995).

[20] Z.-Y. Cheng, M. T. Currie, C. W. Leitz, G. Taraschi, E. A. Fitzgerald, J. L. Hoyt, and D. A. Antoniadas, IEEE Electron Device Lett. **22**, 321 (2001).

[21] A. Nylandsted Larsen, A. Mesli, K. Bonde Nielsen, H. Kortegaard Nielsen, L. Dobaczewski, J. Adey, R. Jones, D. W. Palmer, P. R. Briddon, and S. Öberg, Phys. Rev. Lett. **97**, 106402 (2006).

[22] B. G. Svensson, B. Mohadjeri, A. Hallén, J. H. Svensson, and J. W. Corbett, Phys. Rev. B **43**, 2292 (1991).

[23] A. R. Peaker, V. P. Markevich, L. I. Murin, N. V. Abrosimov, and V. V. Litvinov, Mater. Sci. Eng., B **124-125**, 166 (2005).

[24] P. A. Packan, Science **285**, 2079 (1999).

[25] V. Ranki, J. Nissilä, and K. Saarinen, Phys. Rev. Lett. **88**, 105506 (2002).

[26] V. Ranki, K. Saarinen, H. Fage-Pedersen, J. Lundsgaard Hansen, and A. Nylandsted Larsen, Phys. Rev. B **67**, 041201 (2003).

[27] M. Rummukainen, I. Makkonen, V. Ranki, M. J. Puska, K. Saarinen, and H.-J. L. Gossmann, Phys. Rev. Lett. **94**, 165501 (2005).

[28] V. Ranki, A. Pelli, and K. Saarinen, Phys. Rev. B **69**, 115205 (2004).

[29] V. Ranki and K. Saarinen, Phys. Rev. Lett. **93**, 255502 (2004).

[30] S.-L. Sihto, J. Slotte, J. Lento, K. Saarinen, E. V. Monakhov, A. Y. Kuznetsov, and B. G. Svensson, Phys. Rev. B **68**, 115307 (2003).

[31] M. Rummukainen, J. Slotte, K. Saarinen, H. H. Radamson, J. Hållstedt, and A. Y. Kuznetsov, Phys. Rev. B **73**, 165209 (2006).

[32] L. C. Kimerling, in *Radiation Effects in Semiconductors*, Vol. 31 of *Institute of Physics Conference Series*, edited by N. B. Urli and J. W. Corbett (Institute of Physics, Bristol, 1977), p. 221.

[33] G. D. Watkins and J. W. Corbett, Phys. Rev. **134**, A1359 (1964).

[34] S. D. Brotherton and P. Bradley, J. Appl. Phys. **53**, 5720 (1982).

[35] J. Fage-Pedersen, A. Nylandsted Larsen, and A. Mesli, Phys. Rev. B **62**, 10116 (2000).

[36] E. V. Monakhov, A. Y. Kuznetsov, and B. G. Svensson, J. Appl. Phys. **87**, 4629 (2000).

[37] E. V. Monakhov, A. Y. Kuznetsov, and B. G. Svensson, Phys. Rev. B **63**, 245322 (2001).

[38] P. Kringhøj and A. Nylandsted Larsen, Phys. Rev. B **52**, 16333 (1995).

[39] K. Pennanen, V. Ranki, and K. Saarinen, Physica B **376**, 189 (2006).

[40] N. Cowern and C. Rafferty, MRS Bull. **25**, 39 (2000).

[41] M. D. Giles, Appl. Phys. Lett. **62**, 1940 (1993).

[42] M. D. Giles, J. Electrochem. Soc. **138**, 1160 (1991).

[43] P. Fahey, G. Barbuscia, M. Moslehi, and R. W. Dutton, Appl. Phys. Lett. **46**, 784 (1985).

[44] H.-J. Gossmann, T. E. Haynes, P. A. Stolk, D. C. Jacobson, G. H. Gilmer, J. M. Poate, H. S. Luftman, T. K. Mogi, and M. O. Thompson, Appl. Phys. Lett. **71**, 3862 (1997).

[45] A. R. Allnatt and A. B. Lidiard, Rep. Prog. Phys. **50**, 373 (1987).

[46] H. Bracht and S. Brotzmann, Mater. Sci. Semicond. Process. **9**, 471 (2006).

[47] C. Janke, R. Jones, S. Öberg, and P. R. Briddon, Phys. Rev. B **75**, 195208 (2007).

[48] F. Poulin and J. Bourgoin, Rev. Phys. Appl. (Paris) **15**, 15 (1980).

[49] P. M. Mooney, F. Poulin, and J. C. Bourgoin, Phys. Rev. B **28**, 3372 (1983).

[50] P. A. Stolk, H.-J. Gossmann, D. J. Eaglesham, D. C. Jacobson, C. S. Rafferty, G. H. Gilmer, M. Jaraíz, J. M. Poate, H. S. Luftman, and T. E. Haynes, J. Appl. Phys. **81**, 6031 (1997).

[51] L. Pelaz, M. Jaraiz, G. H. Gilmer, H.-J. Gossmann, C. S. Rafferty, D. J. Eaglesham, and J. M. Poate, Appl. Phys. Lett. **70**, 2285 (1997).

[52] S. Mirabella, E. Bruno, F. Priolo, D. De Salvador, E. Napolitani, A. V. Drigo, and A. Carnera, Appl. Phys. Lett. **83**, 680 (2003).

[53] D. De Salvador, E. Napolitani, G. Bisognin, A. Carnera, E. Bruno, S. Mirabella, G. Impellizzeri, and F. Priolo, Appl. Phys. Lett. **87**, 221902 (2005).

[54] E. Bruno, S. Mirabella, F. Priolo, K. Kuitunen, F. Tuomisto, J. Slotte, F. Giannazzo, C. Bongiorno, V. Raineri, and E. Napolitani, J. Vac. Sci. Technol., B **26**, 386 (2008).

[55] S. Mirabella, E. Bruno, F. Priolo, F. Giannazzo, C. Bongiorno, V. Raineri, E. Napolitani, and A. Carnera, Appl. Phys. Lett. **88**, 191910 (2006).

[56] E. Bruno, S. Mirabella, F. Priolo, E. Napolitani, C. Bongiorno, and V. Raineri, J. Appl. Phys. **101**, 023515 (2007).

[57] E. Bruno, S. Mirabella, E. Napolitani, F. Giannazzo, V. Raineri, and F. Priolo, Nucl. Instrum. Methods Phys. Res., Sect. B **257**, 181 (2007).

[58] C. C. Griffioen, J. H. Evans, P. C. De Jong, and A. van Veen, Nucl. Instrum. Methods Phys. Res., Sect. B **27**, 417 (1987).

[59] V. Raineri, M. Saggio, and E. Rimini, J. Mater. Res. **15**, 1449 (2000).

[60] V. Raineri and S. U. Campisano, Appl. Phys. Lett. **69**, 1783 (1996).

[61] V. Raineri, G. Fallica, and S. Libertino, J. Appl. Phys. **79**, 9012 (1996).

[62] E. V. Monakhov, B. G. Svensson, M. K. Linnarsson, A. L. Magna, M. Italia, V. Privitera, G. Fortunato, M. Cuscunà, and L. Mariucci, Appl. Phys. Lett. **87**, 192109 (2005).

[63] D. K. Schroder, *Semiconductor material and device characterization*, 2nd ed. (John Wiley & Sons, Inc., New York, 1998).

[64] D. V. Lang, Journal of Applied Physics **45**, 3023 (1974).

[65] P. M. Mooney, in *Identification of Defects in Semiconductors*, edited by M. Stavola (Academic Press, San Diego, 1999), Vol. 51B, p. 93.

[66] G. D. Watkins, Phys. Solid State **41**, 746 (1999).

[67] G. D. Watkins, in *Identification of Defects in Semiconductors*, edited by M. Stavola (Academic Press, San Diego, 1998), Vol. 51A, p. 1.

[68] G. D. Watkins, Mater. Sci. Semicond. Process. **3**, 227 (2000).

[69] M. Manninen and R. M. Nieminen, Appl. Phys. A **26**, 93 (1981).

[70] P. Asoka-Kumar, M. Alatalo, V. J. Ghosh, A. C. Kruseman, B. Nielsen, and K. G. Lynn, Phys. Rev. Lett. **77**, 2097 (1996).

[71] I. Makkonen, M. Hakala, and M. J. Puska, Phys. Rev. B **73**, 035103 (2006).

[72] I. Makkonen and M. J. Puska, Phys. Rev. B **76**, 054119 (2007).

[73] K. Saarinen, J. Nissilä, H. Kauppinen, M. Hakala, M. J. Puska, P. Hautojärvi, and C. Corbel, Phys. Rev. Lett. **82**, 1883 (1999).

[74] H. Kauppinen, C. Corbel, K. Skog, K. Saarinen, T. Laine, P. Hautojärvi, P. Desgardin, and E. Ntsoenzok, Phys. Rev. B **55**, 9598 (1997).

[75] A. Calloni, A. Dupasquier, R. Ferragut, P. Folegati, M. M. Iglesias, I. Makkonen, and M. J. Puska, Phys. Rev. B **72**, 054112 (2005).

[76] J. J. Goubet, D. Stievenard, D. Mathiot, and M. Zazoui, Phys. Rev. B **46**, 10113 (1992).

[77] J. Mäkinen, P. Hautojärvi, and C. Corbel, J. Phys. Cond. Matter **4**, 5137 (1992).

[78] V. P. Markevich, I. D. Hawkins, A. R. Peaker, K. V. Emtsev, V. V. Emtsev, V. V. Litvinov, L. I. Murin, and L. Dobaczewski, Phys. Rev. B **70**, 235213 (2004).

[79] V. P. Markevich, private communication, 2007.

[80] V. Torres, private communication, 2008.

[81] M. J. Puska, in *Positron Annihilation*, ICPA 8, edited by L. Dorikens-Vanpraet, M. Dorikens, and D. Segers (World Scientific, Singapore, 1989), p. 101.

[82] R. Würschum, W. Bauer, K. Maier, A. Seeger, and H.-E. Schaefer, J. Phys.: Cond. Matter **1**, SA33 (1989).

[83] P. Moser, J. L. Pautrat, C. Corbel, and P. Hautojärvi, in *Positron Annihilation*, ICPA 7, edited by P. C. Jain, R. M. Singru, and K. P. Gopinathan (World Scientific, Singapore, 1985), p. 733.

[84] C. Corbel, P. Moser, and M. Stucky, Ann. Chim. (Paris) **10**, 733 (1985).

[85] M. J. Puska and R. M. Nieminen, J. Phys. F **13**, 333 (1983).

[86] M. J. Puska and C. Corbel, Phys. Rev. B **38**, 9874 (1988).

[87] M. Saito and A. Oshiyama, Phys. Rev. B **53**, 7810 (1996).

[88] V. P. Markevich, Mater. Sci. Semicond. Process. **9**, 589 (2006).

[89] G. Mannino, V. Privitera, A. La Magna, E. Rimini, E. Napolitani, G. Fortunato, and L. Mariucci, Appl. Phys. Lett. **86**, 051909 (2005).